JCB Journal of Cell Biology

ARTICLE

A molecular mechanism for the procentriole recruitment of Ana2

Tiffany A. McLamarrah[1], Sarah K. Speed[2], John M. Ryniawec[1], Daniel W. Buster[1], Carey J. Fagerstrom[2], Brian J. Galletta[2], Nasser M. Rusan[2]*, and Gregory C. Rogers[1]*

During centriole duplication, a preprocentriole forms at a single site on the mother centriole through a process that includes the hierarchical recruitment of a conserved set of proteins, including the Polo-like kinase 4 (Plk4), Ana2/STIL, and the cartwheel protein Sas6. Ana2/STIL is critical for procentriole assembly, and its recruitment is controlled by the kinase activity of Plk4, but how this works remains poorly understood. A structural motif called the G-box in the centriole outer wall protein Sas4 interacts with a short region in the N terminus of Ana2/STIL. Here, we show that binding of Ana2 to the Sas4 G-box enables hyperphosphorylation of the Ana2 N terminus by Plk4. Hyperphosphorylation increases the affinity of the Ana2–G-box interaction, and, consequently, promotes the accumulation of Ana2 at the procentriole to induce daughter centriole formation.

Introduction

Centrosomes serve as microtubule-nucleating and organizing centers within cells (Conduit et al., 2015). At the core of these organelles lie barrel-shaped centrioles composed of a radial array of nine microtubules (or microtubule bundles) along with several interconnecting proteins (Ito and Bettencourt-Dias, 2018). Centrioles recruit a cloud of pericentriolar material (PCM), which nucleates microtubule growth (Mennella et al., 2014). Position mapping of centrosomal proteins has revealed three hierarchal zones within the organelle that emanate from the centriole center: the centriole, bridge, and PCM zones (Varadarajan and Rusan, 2018). Proteins residing in the bridge zone, such as Sas4/CPAP and Asl/Cep152, are embedded in and/or extend away from the centriole surface and act as scaffolds to recruit and anchor PCM proteins (Fu and Glover, 2012; Lawo et al., 2012; Mennella et al., 2012; Sonnen et al., 2012). Importantly, bridge proteins also play a crucial role in centrosome duplication (Banterle and Gönczy, 2017).

Centrioles are the duplicating elements of centrosomes, a process that is regulated in a cell cycle–dependent manner (Nigg and Holland, 2018). Normally, G1-phase cells contain two centrioles that each spawn an orthogonally positioned "daughter" (also known as a procentriole) during S-phase. During mitotic progression, new daughter centrioles then sequentially recruit the final structural components and bridge proteins needed to produce fully mature centrioles capable of accumulating PCM, thereby enabling them to function as centrosomes in the next cell cycle (Wang et al., 2011). For example, *Drosophila melanogaster* Sas4, which is present on daughter centrioles as cells enter mitosis, is essential for the mitotic loading of its binding partner Asl (Dzhindzhev et al., 2010; Novak et al., 2014; Fu et al., 2016).

Although the earliest physical manifestation of procentrioles appears during S-phase (Robbins et al., 1968), duplication in flies begins during mitosis with the recruitment of the master-regulator Polo-like kinase 4 (Plk4). Plk4 activity is necessary for centriole assembly and is sufficient to induce centriole overduplication when overexpressed in a variety of cell types (Bettencourt-Dias et al., 2005; Habedanck et al., 2005; Kleylein-Sohn et al., 2007; Peel et al., 2007; Rodrigues-Martins et al., 2007; Holland et al., 2010). Initially, Plk4 interacts with a centriole-targeting factor, such as Asl (Cep152 in humans; Cizmecioglu et al., 2010; Dzhindzhev et al., 2010; Hatch et al., 2010; Kim et al., 2013; Sonnen et al., 2013), and, during late mitosis, appears on each mother centriole as a single asymmetric spot, a structure called the "preprocentriole" from which the daughter centriole assembles (Dzhindzhev et al., 2017). Characterizing the functional consequences of Plk4's phosphorylation of multiple substrates is key to understanding centriole assembly.

[1]Department of Cellular and Molecular Medicine, University of Arizona Cancer Center, University of Arizona, Tucson, AZ; [2]National Heart, Lung, and Blood Institute, National Institutes of Health, Bethesda, MD.

*N.M. Rusan and G.C. Rogers contributed equally to this paper; Correspondence to Nasser M. Rusan: Nasser.rusan@nih.gov; Gregory C. Rogers: gcrogers@email.arizona.edu.

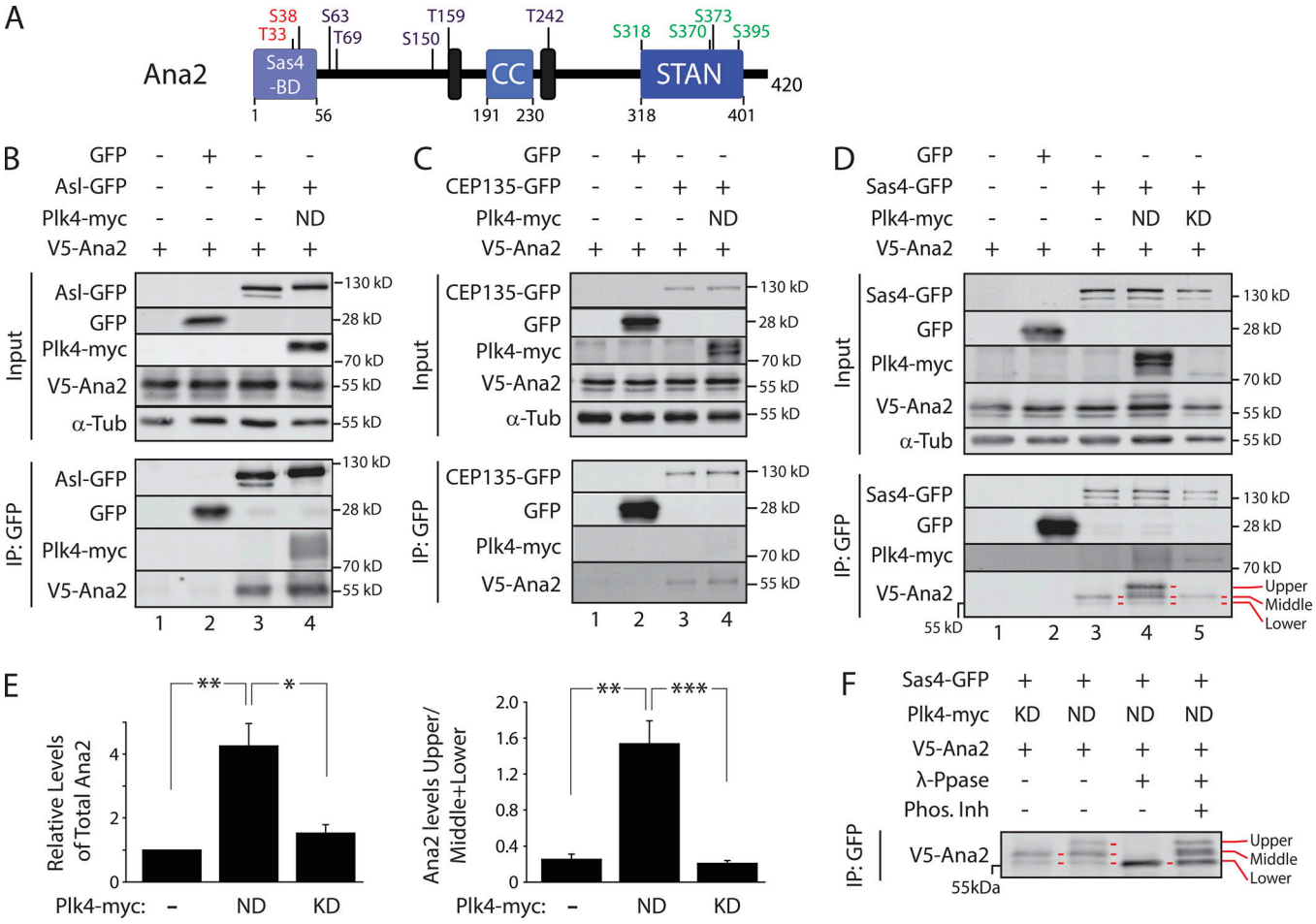

Figure 1. **Plk4 activity enhances the interaction between Ana2 and Sas4, producing a hyperphosphorylated Ana2 species. (A)** Linear map of Ana2 depicting functional domains and Plk4 phospho-sites. Ana2 is phosphorylated by Plk4 in an ordered pattern, first on NT residues T33/S38 (red) followed by STAN domain residues S318/S370/S373/S395 (green), and then central residues S63/T69/S150/T159/T242 (purple; McLamarrah et al., 2018). Sas4-binding domain (BD; Cottee et al., 2013), LC8 binding-sites (black boxes; Slevin et al., 2014), coiled coil (CC), and STAN domains are shown. **(B–D)** Ana2 binds Cep135 (B), Asl (C), and Sas4 (D), but coexpression of catalytically active ND Plk4 enhances only the association with Sas4. S2 cells were cotransfected with the indicated constructs and the next day induced to express for 24 h by the addition of 1 mM $CuSO_4$. Anti-GFP IPs were then prepared from lysates, and Western blots of the inputs and 5% of the IPs probed for GFP, V5, myc, and α-tubulin. Note Ana2 presents as three different phospho-species (red lines in all figures) indicated as lower (nonphospho), middle (phospho), and upper (hyperphospho) species. Coexpression of active Plk4 (but not KD) and Sas4 generates a hyperphospho-Ana2 species (D). **(E)** Graphs show relative Ana2 intensities from IPs like D, lanes 3–5. Left: Ana2 intensities within a region of interest containing all Ana2 species were measured and normalized to the treatment lacking Plk4 expression. Right: Graph shows ratio of the upper (hyperphosphorylated) to the middle and lower Ana2 species for the three indicated treatments. Asterisks mark significant differences between treatments: *, $P < 0.05$; **, $P < 0.01$; ***, $P < 0.001$. Error bars, SEM; $n = 3$ (left panel) and 6 (right panel) experiments. **(F)** Coexpression of active Plk4 and Sas4 generates a hyperphosphorylated form of Ana2. Anti-GFP IPs were prepared from cell lysates expressing the indicated proteins and then were either mock-treated (lanes 1 and 2) or incubated with λ-phosphatase (λ-Ppase; lane 3) or λ-phosphatase plus phosphatase inhibitor cocktail (Phos. Inh; lane 4).

Drosophila Anastral Spindle 2 (Ana2; STIL in humans) is an essential centriole zone protein (Goshima et al., 2007) and co-localizes with Plk4 on preprocentrioles. Ana2 contains an N-terminal (NT) Sas4 binding domain, a central coiled-coil, and a C-terminal STil/ANa2 (STAN) domain (Fig. 1 A; Stevens et al., 2010; Tang et al., 2011; Vulprecht et al., 2012; Cottee et al., 2013; Hatzopoulos et al., 2013). Through interactions with its coiled-coil and C terminus, Ana2/STIL binds Plk4 (Dzhindzhev et al., 2014; Ohta et al., 2014, 2018; Kratz et al., 2015; McLamarrah et al., 2018), and activates the kinase, possibly by relieving Plk4 autoinhibition (Klebba et al., 2015; Arquint et al., 2015; Moyer et al., 2015). In turn, Ana2/STIL is extensively phosphorylated (Dzhindzhev et al., 2014; Ohta et al., 2014; Kratz et al., 2015), which occurs in an ordered pattern (Fig. 1 A; McLamarrah et al., 2018). Initially, phosphorylation predominantly occurs in the N terminus, which promotes Ana2 recruitment to the procentriole assembly site (Dzhindzhev et al., 2017). Subsequently, phosphorylation of the STAN domain generates a phospho-binding site for the cartwheel protein, Sas6, a critical step required for Sas6 procentriole loading (Dzhindzhev et al., 2014; Ohta et al., 2014; Kratz et al., 2015; Moyer et al., 2015). Last, phosphorylation of the Ana2 central region releases Plk4 (McLamarrah et al., 2018).

While the mechanism of Sas6 recruitment to the pre-procentriole appears well established, the mechanism executing the preceding assembly step, Ana2 recruitment, is still obscure.

Based on the finding that deletion of the central coiled-coil in Ana2 prevents Plk4 binding and targeting to centrioles (Ohta et al., 2014; Arquint et al., 2015; Kratz et al., 2015; Moyer et al., 2015), it has been proposed that a direct interaction with Plk4 mediates Ana2 loading onto centrioles. However, we have shown that coiled-coil deletion actually has multiple deleterious effects because it also disrupts Ana2's ability to oligomerize and interact with Sas4 (McLamarrah et al., 2018). By using a separation-of-function phosphomimetic (PM) mutation in Ana2 that is unable to bind Plk4, we observed that PM Ana2 localizes properly to the procentriole assembly site (McLamarrah et al., 2018), suggesting that Ana2 recruitment relies on a mechanism independent of Plk4 binding. Importantly, though, Ana2/STIL localization to centrioles requires Plk4 kinase activity (Moyer et al., 2015; Dzhindzhev et al., 2017), consistent with the observation that phosphorylation of the Ana2 N terminus is necessary for procentriole recruitment. How Ana2 phosphorylation promotes its targeting to the procentriole assembly site is unknown. Here, we provide evidence for the first molecular mechanism of Ana2 recruitment, a multiple step process coordinated through Sas4 to achieve Ana2 enrichment on the procentriole assembly site.

Results

Sas4 promotes Ana2 hyperphosphorylation by Plk4

Drosophila Ana2 does not require direct binding to Plk4 for its recruitment to procentrioles (McLamarrah et al., 2018). However, centriole recruitment of Ana2/STIL does require Plk4 kinase activity as well as phosphorylation of Ana2's N terminus (Moyer et al., 2015; Dzhindzhev et al., 2017). Therefore, we hypothesized that Plk4 activity enhances the interaction between Ana2 and a protein that resides at or near the centriole surface. Cep135, Asl, and Sas4 are excellent candidates because they fulfill this spatial criterion and are also known to directly bind Ana2 (Cottee et al., 2013; Hatzopoulos et al., 2013; Galletta et al., 2016). To test whether Plk4 activity increases the association of Ana2 with these proteins, we coexpressed a highly active, nondegradable (ND) form of Plk4-myc with V5-Ana2 in S2 cells along with GFP-tagged Asl, Cep135, or Sas4. We then performed GFP immunoprecipitations (IP) and examined the amount of V5-Ana2 in the immunoprecipitate. As expected, Ana2 associated with all three proteins without Plk4 overexpression, but not control GFP (Fig. 1, B–D, lanes 1–3). In cells coexpressing Plk4, we found that Ana2 levels remained unchanged in Asl and Cep135 IPs (Fig. 1, B and C, lanes 4). However, coexpressed active (ND) Plk4 promoted a fourfold increase in the total amount of Ana2 that associated with Sas4 (Fig. 1, D [lane 4] and E, left panel). Notably, this effect required Plk4 kinase activity because Ana2 enrichment was not observed from cells coexpressing kinase-dead (KD) Plk4 (Fig. 1, D [lane 5] and E [left panel]).

Closer examination of the immunoblots revealed that Ana2 normally exists as a tight doublet on SDS-PAGE (Fig 1, D, lane 3), suggesting that Ana2 isoforms with differing phosphorylation states are present. Strikingly, Sas4 and Plk4 coexpression shifted some Ana2 to an even slower electrophoretic mobility (Fig. 1 D, lane 4, upper band). This shift in Ana2 mobility was not observed with coexpression of Plk4 and Asl or Cep135 (Fig. 1, B and C), nor was it seen with the combined expression of Sas4 and KD Plk4 (Fig. 1 D), indicating that coexpression of Sas4 and Plk4 leads to a new hyperphosphorylated Ana2 species. This was confirmed by phosphatase treatment of the IPs, which collapsed both middle and upper Ana2 isoforms to the lower nonphosphorylated species; the effect of the phosphatase on collapsing the Ana2 triplet was prevented by addition of phosphatase inhibitor (Fig. 1 F). Moreover, the proportion of hyperphosphorylated Ana2 that bound Sas4 was sevenfold greater when Plk4 was catalytically active compared with cells expressing inactive Plk4 (Fig. 1 E, right panel). Taken together, our findings suggest that Plk4 activity enhances the interaction between Sas4 and Ana2.

Ana2 phosphorylation by Plk4 requires interaction between Ana2 and the Sas4 G-box

We next asked which domain in Sas4 is responsible for the increased binding and production of hyperphosphorylated Ana2 in cells overexpressing Plk4. Sas4 is a multidomain protein containing an NT PN2-3 domain, an adjacent microtubule-binding domain, and a central coiled-coil, and ends with the amyloid-like G-box/TCP domain (Hung et al., 2004; Hsu et al., 2008; Hatzopoulos et al., 2013; Zheng et al., 2014, 2016; Cutts et al., 2015; Sharma et al., 2016). We first carved Sas4 into three regions named A, B, and C (Fig. 2 A) and expressed each as a GFP-fusion along with V5-Ana2 and Plk4-myc (either active or KD) in S2 cells. As before, GFP IPs were performed to analyze for differences in Ana2 binding and mobility on SDS-PAGE. We found that only the G-box (Sas4-C) was sufficient for Ana2 binding (Fig. 2 B, lanes 9 and 10). In addition, Ana2 bound the G-box regardless of expressed Plk4 activity (Fig. 2 B, lanes 3 vs. 4 and 9 vs. 10). These results confirm previous work that found Ana2/STIL N terminus bound the G-box regardless of its phosphostate (Cottee et al., 2013; Hatzopoulos et al., 2013). Notably, expression of active Plk4 did have two effects: active Plk4 generated hyperphosphorylated Ana2 and increased the proportion of this species in the IP (Fig. 2 B, inputs, lanes 3 vs. 4 and 9 vs. 10; and Fig. 2 C). Expression of a truncated Sas4 mutant lacking the G-box (ΔC) failed to bind Ana2 (Fig. 2 B, lanes 11 and 12). Thus, within the context of this assay, our findings suggest that the Sas4 G-box by itself is necessary and sufficient for Plk4 to hyperphosphorylate Ana2 and enhance the Ana2–Sas4 interaction.

Previous work revealed that the Sas4–Ana2 interaction is highly conserved, and structural studies of the complex show direct binding between a short segment of the Ana2 N terminus and the single β-sheet comprising the G-box (Cottee et al., 2013; Hatzopoulos et al., 2013). This interaction is clearly important: G-box mutations that disrupt Ana2 binding prevent centriole duplication and are linked to primary microcephaly (Thornton and Woods, 2009; Cottee et al., 2013). Although a structural role within the cartwheel has been proposed for the Ana2–G-box interaction, at present it is unknown how this interaction promotes centriole assembly at a mechanistic level. Therefore, we asked whether disrupting the Ana2–G-box interaction could prevent Plk4 from phosphorylating Ana2. Based on the atomic structure of the fly complex (Cottee et al., 2013), we made

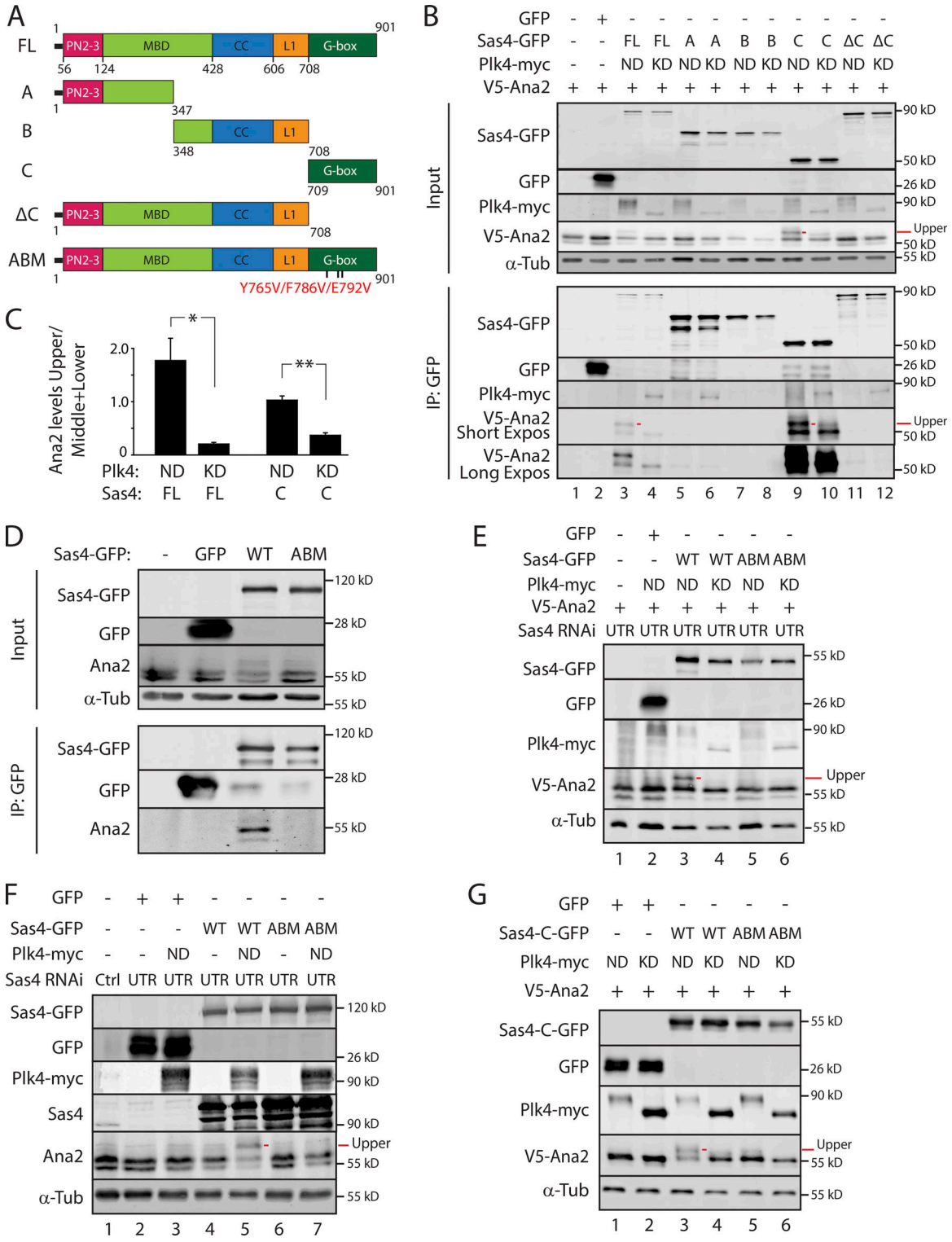

Figure 2. **Binding between Ana2 and the Sas4 G-box is required for Plk4-dependent phosphorylation of Ana2 and for enhanced Ana2-Sas4 association. (A)** Linear maps of Sas4 constructs used in these experiments. PN2-3, tubulin-binding domain; MBD, microtubule-binding domain; CC, coiled-coil; L1, linker 1. The ABM harbors the indicated amino acid substitution (Bond et al., 2005; Cottee et al., 2013). **(B)** Sas4 G-box promotes hyperphosphorylation of Ana2 by Plk4. S2 cells were treated as described in Fig. 1 B. Anti-GFP IPs were then prepared from lysates, and Western blots of the inputs and IPs probed for GFP, V5, and myc. The hyperphosphorylated Ana2 isoform is clearly diminished in the presence of KD Plk4 or absence of the Sas4 G-box (Sas4-C). Note, G-box (lanes 9 and 10) expression is much higher than FL (lanes 3 and 4) Sas4 and thus binds proportionally more Ana2. **(C)** Graph shows the ratios of the band intensities of the upper (hyperphosphorylated) to the middle + lower Ana2 species for the indicated treatments (like lanes 3 vs. 4 and 9 vs. 10 in B). Asterisks mark significant differences between treatments: *, $P < 0.05$; **, $P < 0.01$. Error bars, SEM; $n = 3$ experiments. **(D)** Endogenous Ana2 does not coIP with Sas4 containing the ABM. S2 cells were depleted of endogenous Sas4 by targeting its UTR for 12 d. On days 4 and 8, cells were transfected with the indicated constructs and

induced to express the next day for the duration of the experiment by the addition of 1 mM $CuSO_4$. Anti-GFP IPs were then prepared from lysates, and Western blots of the inputs and IPs probed for GFP, Ana2, and α-tubulin. **(E and F)** An ABM in the Sas4 G-box disrupts hyperphosphorylation of transgenic (D) and endogenous (E) Ana2 by Plk4. S2 cells were depleted of Sas4 by RNAi targeting its UTR for 6 d. On day 4, cells were transfected with the indicated constructs and induced to express the next day for 24 h by the addition of 1mM $CuSO_4$. Blots of cell lysates were probed with anti-GFP, V5, myc, Ana2, and α-tubulin. Note that hyperphosphorylated Ana2 is absent when endogenous Sas4 is replaced with Sas4-ABM. **(G)** Expression of Sas4-C (G-box) harboring the ABM prevents the electrophoretic shift in transgenic Ana2. S2 cells were treated as in A. Proteins were detected by immunoblotting cell lysates with anti-GFP, myc, V5, and α-tubulin.

substitutions in three key G-box residues (Y765V/F786V/E792V) designed to specifically abolish Ana2 binding, which included the microcephaly equivalent mutation E792V (E1235V in human Sas4; Bond et al., 2005). We named this the Ana2-binding mutant (ABM; Fig. 2 A). Endogenous Sas4 was depleted from S2 cells using RNAi and then replaced with GFP, full-length (FL) WT Sas4-GFP, or Sas4-ABM-GFP. Whereas endogenous Ana2 coimmunoprecipitated (coIPed) with Sas4-WT, it did not associate with Sas4-ABM (Fig. 2 D). Notably, V5-Ana2 was hyperphosphorylated when active Plk4 was coexpressed with Sas4-WT (Fig. 2 E, lane 3) but not when Sas4 was absent (Fig. 2 E, lane 2) or when the binding mutant, Sas4-ABM, was coexpressed (Fig. 2 E, lane 5). Similarly, endogenous Ana2 was hyperphosphorylated in the presence of active Plk4 when Sas4-WT (but not Sas4-ABM) was expressed (Fig. 2 F). Last, expression of the Sas4-C fragment containing the ABM mutations also failed to hyperphosphorylate Ana2 when coexpressed with active Plk4 (Fig. 2 G). Taken together, our findings provide the first mechanistic insight into the conserved Ana2–G-box interaction, namely that it enables Plk4 to phosphorylate Ana2, which then enhances Ana2 binding to Sas4.

The Sas4 G-box binds the Plk4 polo box 1–2 cassette

How does the Sas4 G-box facilitate Plk4 phosphorylation of Ana2? One possibility is that the G-box, which forms a single extended β-sheet (Cutts et al., 2015), acts as a binding platform for both Plk4 and Ana2, placing them in a proximity and orientation that stimulates Ana2 phosphorylation. However, direct binding between Sas4 and Plk4 has not been shown and was not previously detected in our yeast two-hybrid (Y2H) map of the fly centrosome (Galletta et al., 2016). To identify new interactions between fly centrosome proteins, we developed a high-throughput protein screen for proteins that form stable binary complexes in bacteria. 17 centrosome genes were selected for analysis, including Sas4, Plk4, and Ana2 (Fig. 3, A and B). FL genes and fragments were randomly inserted into a bacterial dual-tag expression plasmid where one component is tagged with either His_6 and the other with GFP (Fig. 3, C and C′; and Table S1). In brief, bacterial lysates were subjected to a two-step affinity-purification scheme to isolate protein complexes. From 992 isolated bacterial colonies, we identified 90 bacterial lysates containing both His_6 and GFP proteins (Fig. 4 A and Fig. S1). False-positive dual-tagged single proteins were eliminated by PCR analysis, as well as duplicate dual protein expression vectors, leaving a possible 48 positive interactors (Fig. 4 A, 2a and 2b). Binding was further tested by scaling up the cultures and using a secondary screen consisting of tandem His_6 pull-down followed by GFP IP, resulting in 21 positive interactions (Fig. 4 A, 2c; Fig. S2; and Supplemental immunoblot PDF). These interactions were subjected to a final GFP IP step to test for reciprocal binding, yielding six high-confidence interactors (Fig. 4 A, 2d; and Fig 4, B and B′). These included (1) the central Plk4 Polo box (PB) cassette PB1-PB2 with itself, (2) PB1-PB2 and the N terminus of Asl, and (3) NT and C-terminal fragments of Ana2; all three are well-described interactions that validated our screen (Slevin et al., 2012; Dzhindzhev et al., 2010; McLamarrah et al., 2018). Remarkably, we also identified the Sas4 G-box as another PB1-PB2 binding partner as well as an interaction between the G-box and a C-terminal fragment of Ana2 lacking the previously described G-box–binding motif. (An interaction between the Ana2 N terminus and Cnn was also detected but is not examined further in this study.) We note that G-box/PB1-PB2 binding was not preserved during the tandem GFP-IP step of the screen, indicating that this interaction is weaker compared with the other interactors.

To further test the direct interaction between Sas4 and Plk4, we purified recombinant maltose-binding protein (MBP)–tagged G-box (Sas4 amino acids 708–901) as well as partially purified His_6-PB1-PB2 (Plk4 amino acids 382–602; Fig. 4 C), which we fluorescently labeled. Binding affinity between the proteins was then measured using microscale thermophoresis (MST), which analyzes protein–protein interactions in complex mixtures where only one species is fluorescently labeled (Jerabek-Willemsen et al., 2011). This analysis confirmed binding between the G-box and PB1-PB2 with a K_d = 28.2 μM; no binding was detected between control MBP and PB1-PB2 (Fig. 4 D). Taken together, our findings suggest that Plk4 directly binds the Sas4 G-box through its PB1-PB2 cassette with relatively low affinity, and that Ana2 may contain additional undescribed G-box binding sites.

Sas4 promotes Plk4 phosphorylation of Ana2 S38

We next sought to determine which Ana2 residues are primarily phosphorylated in the presence of Sas4. Several potential sites exist, as Ana2 is phosphorylated by Plk4 on at least 11 residues along its length (Fig. 1 A; Dzhindzhev et al., 2014; McLamarrah et al., 2018). It follows that substitution of the relevant Ana2 Ser/Thr residues with nonphosphorylatable alanine (A) would block the shift in Ana2 mobility when coexpressed with Sas4 and Plk4, whereas PM Asp/Glu substitutions would produce electrophoretic shifts in cells containing inactive Plk4. We first examined whether Sas4 promotes Plk4 phosphorylation of Ana2's STAN domain. Although modification of this region is not required for centriole targeting in fly cells (Dzhindzhev et al., 2014), it does control the localization of STIL in cultured human cells (Moyer et al., 2015). Therefore, we made substitutions of the three most conserved phosphorylated STAN residues (S318/S370/S373; generating nonphosphorylatable "3A" and PM "3PM" mutants)

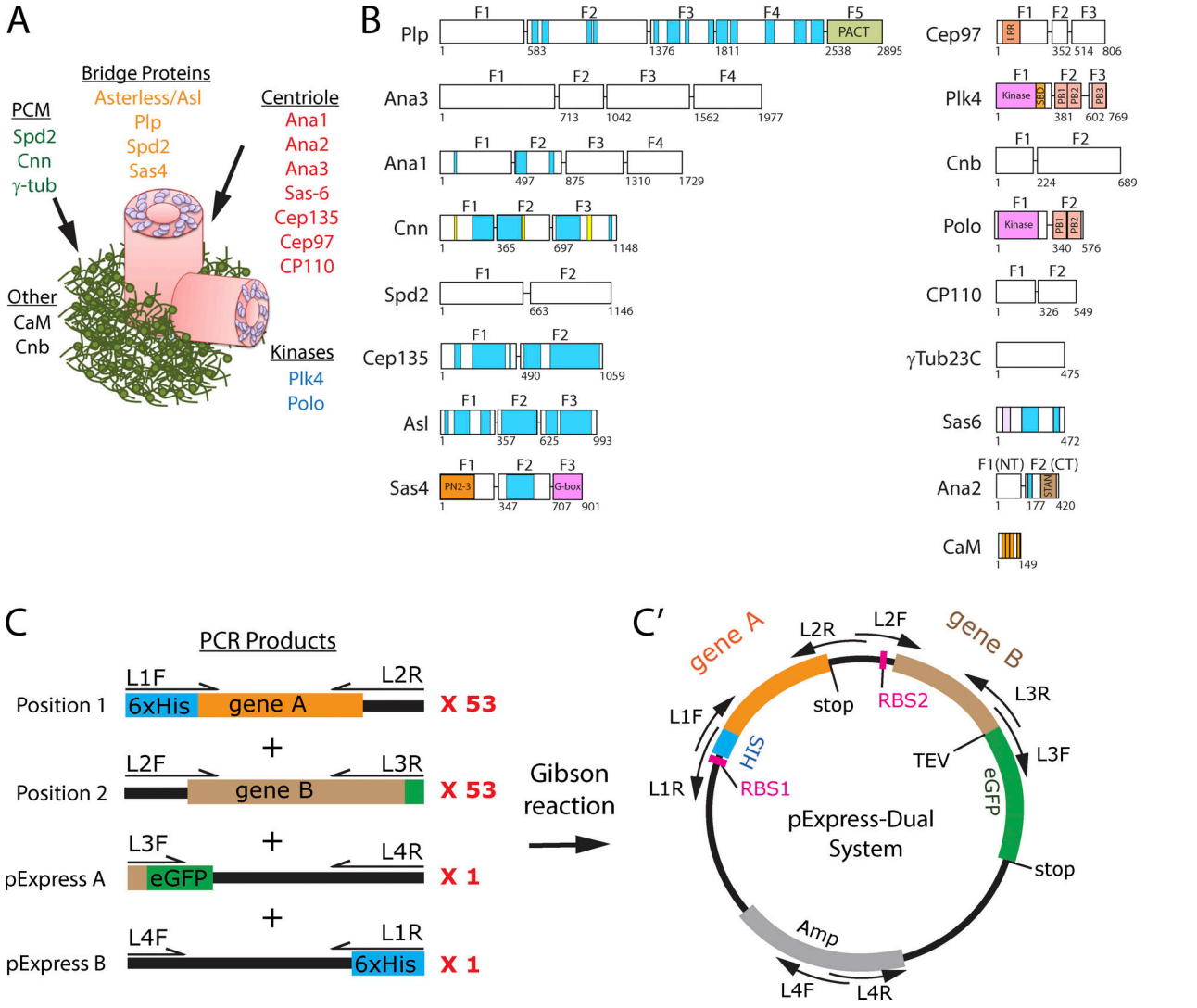

Figure 3. **17 *Drosophila* centrosome proteins were selected for binary complex screening. (A)** Cartoon shows the 17 centrosome proteins that were selected for binary complex solubility screening and their positions within the centrosome. **(B)** Schematic of the proteins tested in the screen. Numbers show amino acids, blue regions predict coiled-coils, additional structural/functional domains are indicated, and horizontal lines show the locations where proteins were subdivided into smaller testable fragments (F1–5). Also described in Galletta et al. (2016). **(C)** PCR products used for random plasmid assembly. Each gene was amplified as FL and/or sub-fragments using primers listed in Table S2. L1F and L2R primers were used to generate 53 unique PCR products that could occupy the "gene A" position. L2F and L3R primers were used to generate 53 unique PCR products that could occupy the "gene B" position. pExpress A and B PCR fragments were used to assemble the plasmid backbone. **(C′)** Schematic of the final plasmid indicating the positions of the His_6-geneA and geneB-GFP, primers, and the ribosome binding sites (RBS1 and RBS2).

and then examined V5-Ana2 mobility by Western blotting Sas4-GFP IP samples. Both Ana2-3A and 3PM coIPed with Sas4 and shifted to slower migrating isoforms in cells coexpressing active Plk4 (Fig. 5 A, lanes 5 and 7), demonstrating that STAN domain phosphorylation is not responsible for the Sas4-dependent shift in Ana2 mobility.

We next tested whether Sas4 promotes phosphorylation of Ana2's N terminus by examining mutants with substitutions (A "2A," or glu/asp "2PM") of both phospho-residues T33 and S38 (Fig. 1 A). We found that, despite its ability to coIP with Sas4, Ana2-2A failed to shift to the hyperphosphorylated isoform, and its levels did not increase in the immunoprecipitates when coexpressed with active Plk4 (Fig. 5 B, lanes 5 and 6). In contrast, Ana2-2PM produced the mobility shift regardless of Plk4's catalytic state (Fig. 5 B, lanes 7 and 8). Thus, Sas4 increases the Plk4-dependent phosphorylation of Ana2's N terminus.

To determine whether Ana2's mobility shift and enhanced binding to Sas4 were due to modification of a single residue, we generated individual T33 and S38 phospho mutants and, as before, examined their mobilities by Western blotting Sas4-GFP IP samples. We found that only one mutation, S38A, prevented the Ana2 mobility shift in immunoprecipitates when coexpressed with Sas4 and active Plk4 (Fig. 5 C, lanes 9 and 10). PM S38D displayed the mobility shift regardless of Plk4 activity (Fig. 5 C, lanes 11 and 12), but did not consistently accumulate in the IP; likely this mutant does not act as a perfect PM. Identical changes in Ana2 mobility were also detected in whole lysates prepared from cells depleted of endogenous Ana2 (Fig. 5 D). Our data

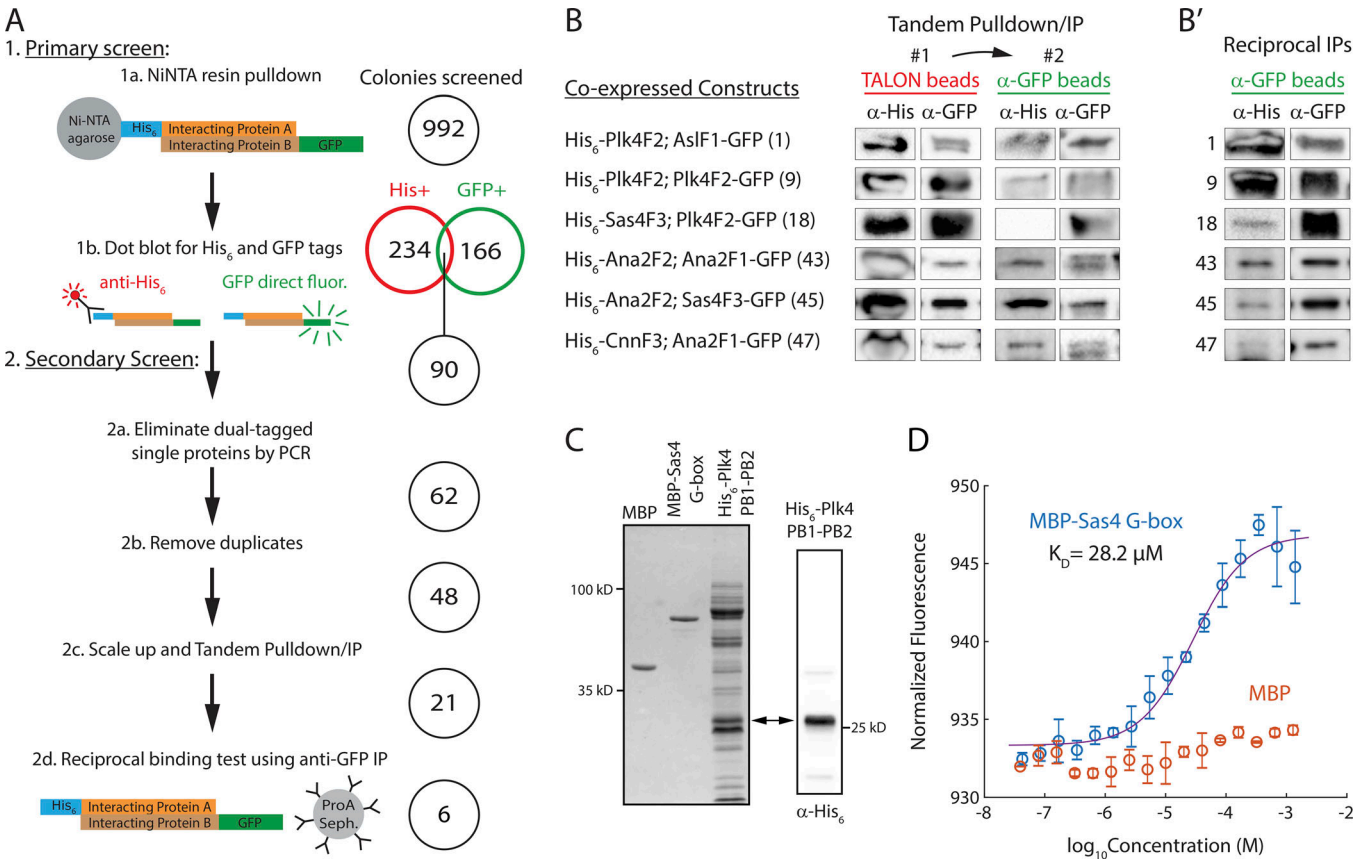

Figure 4. **A dual-expression screen of Drosophila centrosome proteins identifies 6 soluble binary protein complexes. (A)** Summary of screen and results. A total of 992 colonies were cultured and processed as described. (1a and 1b) The screen was conducted in two steps. Primary screening used Ni-NTA pulldowns followed by immuno-dot blots to detect His and GFP-tagged protein, resulting in 90 binary complexes. The secondary screen consisted of four steps: (2a) PCR was used to eliminate individual proteins that were dual tagged with both His and GFP and (2b) to remove duplicate plasmids. (2c) Cultures were scaled up for tandem pulldown/IP using first Ni-NTA and then GFP antibodies. Finally, (2d) the 21 positive interactions were verified with a reciprocal IP using anti-GFP. **(B and B′)** Six protein complexes were identified using the pExpress-Dual screen, which involved a tandem His_6-pulldown/GFP-IP (B) and a final reciprocal GFP-IP step (B′). Immunoblots were probed with the indicated anti-His and GFP antibodies. The IP interaction numbers are the same as those in Fig. S2 B. Complexes 1, 9, and 43 were previously identified by other studies and serve as a strong proof of concept (Dzhindzhev et al., 2010; Slevin et al., 2012; McLamarrah et al., 2018). Interactions 18 and 45 are the subject of this study. Interaction 47 is a novel interaction. Note, G-box/PB1-PB2 binding is not preserved through the second GFP-IP step of the tandem pulldown/IP (interaction 18), demonstrating the relative low affinity of this interaction. **(C)** Left: Coomassie-stained SDS-PAGE showing purified MBP, MBP-Sas4 G-box, and partially purified His_6-Plk4 PB1-PB2. Arrow indicates the position of His_6-Plk4 PB1-PB2. Right: Immunoblot of the partially purified His_6-Plk4 PB1-PB2 sample probed with anti-His_6 antibody. **(D)** Binding isotherms derived from MST experiments. The His_6-Plk4 PB1-PB2 concentration (50 mM) was constant in all experiments. The concentration of MBP and MBP-Sas4 was varied across more than four orders of magnitude (x axis). No binding of MBP to His_6-PB1-PB2 was observed. Curve-fitting of the binding isotherm for MBP–G-box yielded a K_d of 28.2 μM (log_{10} concentration = −4.55 ± 0.14 M).

indicate that the Ana2–Sas4 interaction is required for Plk4 to phosphorylate Ana2 (Fig. 2, E and F), and failure of the S38A mutant to shift to the slower migrating species could be explained if S38 was required for Sas4 binding. Because Ana2 oligomerizes (Slevin et al., 2014), we again used RNAi to eliminate the influence of endogenous Ana2 on the IP assay. Interestingly, each S38 phospho mutant can bind Sas4 regardless of Plk4 activity (Fig. 5 E, lanes 6–9). Thus, our findings indicate that Sas4 directs Plk4 to phosphorylate S38 of Ana2, although S38 phosphorylation is not required for Ana2 to bind Sas4.

If Ana2-Sas4 binding is required for Ana2 hyperphosphorylation, then a Sas4-binding mutation in Ana2 should also prevent its hyperphosphorylation when coexpressed with Sas4 and active Plk4. To test this, we depleted cells of endogenous Ana2 and replaced it with a P11A/R12A double mutant; P11 and R12 lie in the conserved PRxxPxP motif that directly interacts with the Sas4 G-box, based on the atomic structure of the complex (Cottee et al., 2013; Hatzopoulos et al., 2013). Although an experiment to determine if the double mutation disrupts Sas4 binding was not performed, analogous mutations in zebrafish STIL dramatically decrease Sas4 binding (Cottee et al., 2013). Nevertheless, Ana2-P11A/R12A does not fully rescue centrosome duplication in Ana2 mutant embryos (Cottee et al., 2013). We found that Ana2-P11A/R12A was able to coIP with Sas4 from Ana2-depleted cell lysates but at reduced levels and failed to shift to the hyperphosphorylated form as assayed by Western blotting of whole cell lysates and Sas4-GFP IPs (Fig. 5, D and E, lanes 10 and 11). Thus, our results indicate that an intact PRxxPxP motif is required for Ana2 phosphorylation by Plk4.

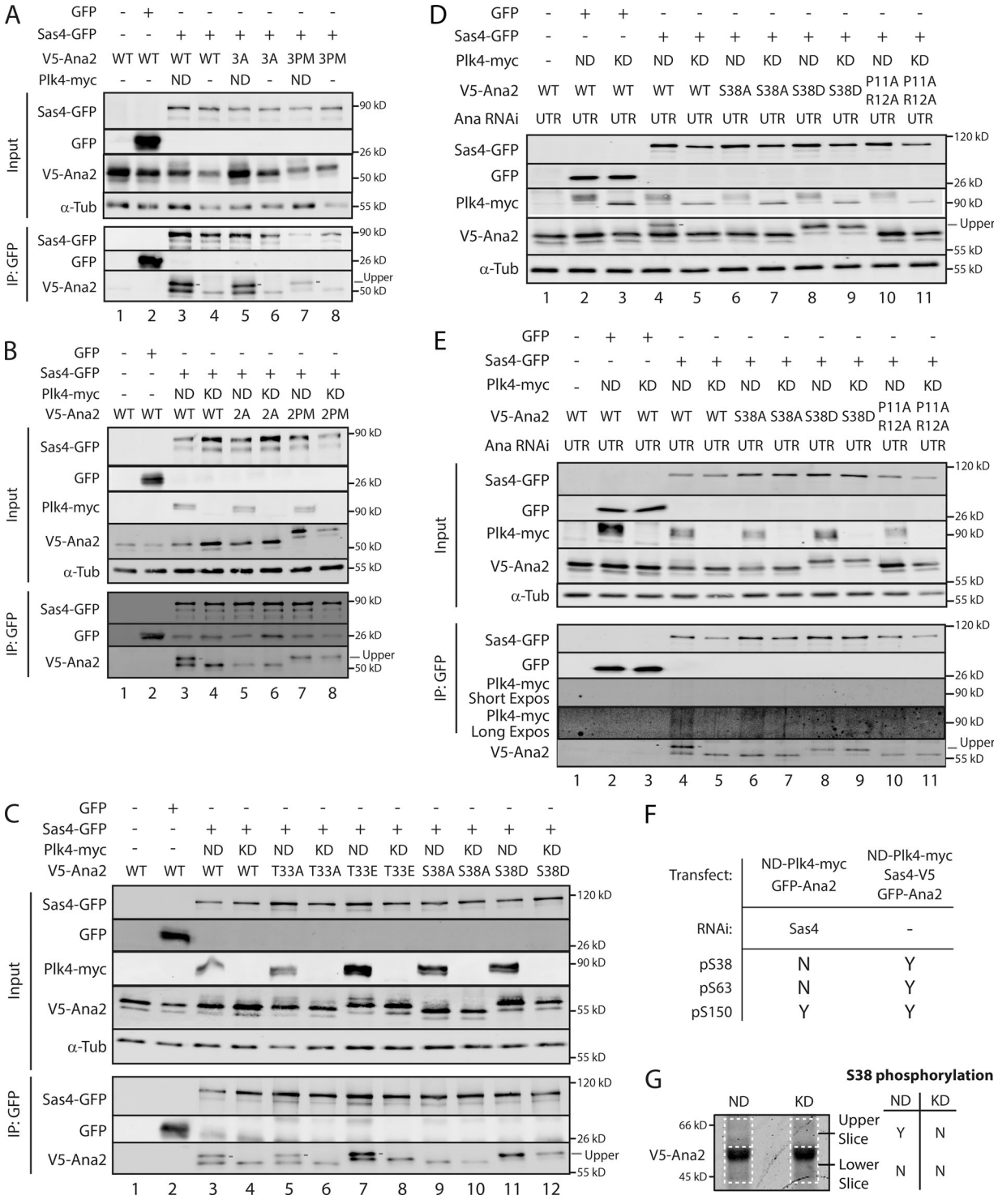

Figure 5. **Sas4 stimulates Plk4 phosphorylation of Ana2 S38. (A)** Phospho-mutations in the STAN domain (3A or 3PM) of Ana2 do not affect the ability of Sas4 and Plk4 to hyperphosphorylate Ana2. S2 cells were cotransfected with the indicated constructs and the next day induced to express for 24 h by addition of 1 mM $CuSO_4$. Anti-GFP IPs were then prepared from lysates, and Western blots of the inputs and IPs probed for GFP, V5, and α-tubulin. **(B)** Double phospho-mutation of NT residues T33 and S38 (2A or 2PM) alter the electrophoretic shift of Ana2. S2 cells were treated as in A. Anti-GFP IPs were then prepared from lysates, and Western blots of the inputs and IPs were probed for GFP, myc, V5, and α-tubulin. **(C)** Phospho-mutations in S38 but not T33 affect the electrophoretic shift of Ana2. S2 cells were treated as in A. Anti-GFP IPs were then prepared from lysates, and Western blots of the inputs and IPs probed for GFP, myc, V5, and α-tubulin. **(D and E)** The phospho-null mutation S38A and the Sas4-binding mutation P11A/R12A prevent the shift in Ana2's electrophoretic mobility. S2 cells were Ana2-depleted by RNAi targeting the UTR for 6 d. On day 4, cells were transfected with the indicated constructs and induced to express the next day for 24 h by the addition of 1 mM $CuSO_4$. Whole cell lysates (D) or anti-GFP IPs (E) were then prepared and Western blots of the samples were probed for GFP, V5, myc, and α-tubulin. **(F)** Table shows the presence (Yes or No) of NT phospho-residues in Ana2 IPed from cells with the indicated treatments. **(G)** Coomassie-stained protein gel of immunoprecipitated Ana2 from S2 cells coexpressing Sas4-GFP and either active (ND) or KD Plk4-myc. Gel slices corresponding to the upper and lower migratory species of Ana2 (dashed lines) were isolated and prepared for MS/MS analysis. Detection (yes or no) of phospho-S38 within each gel region by MS/MS is shown.

Our previous in vitro kinase assays and tandem mass spectrometry (MS/MS) of Ana2 revealed that S38 is one of the first residues phosphorylated by Plk4 (McLamarrah et al., 2018). Curiously, however, we did not detect S38 phosphorylation when Ana2 was purified from cells overexpressing Plk4. Possibly, this is because Sas4 was not cooverexpressed in these cells, whereas the high concentrations of Plk4 and Ana2 of in vitro reactions can overcome the need for Sas4 to facilitate S38 phosphorylation. To explore this hypothesis, we performed MS/MS analysis of Ana2 immuno-purified from cells coexpressing Plk4 and that were either depleted of Sas4 or coexpressing Sas4 (Table S2). Phospho-S38 was not detected in Sas4-depleted cells, although phosphorylation of S150, a different Plk4-targeted residue (Dzhindzhev et al., 2014; McLamarrah et al., 2018), was detected (Fig. 5 F). In contrast, expression of Sas4 resulted in detectable phosphorylated S38, S63, and S150 (Fig. 5 F). We next determined which electrophoretic species of Ana2 contained phospho-S38. Ana2 was immuno-purified from cells expressing Sas4 and either catalytically active (ND) or KD Plk4, the IP samples were resolved by SDS-PAGE, and then the upper and lower sections of the stained gel were analyzed separately by MS/MS (Fig. 5 G, dashed lines mark analyzed sections). Notably, phospho-S38 was only detected in cells coexpressing Sas4 and ND-Plk4 and only in the upper gel slice, where hyperphosphorylated Ana2 migrates. Taken together, our results indicate that Sas4 directs Plk4 to phosphorylate S38 in Ana2, thereby generating the slower migrating Ana2 species.

Phosphorylation of S38 stimulates Ana2 accumulation on procentrioles

In *Drosophila* cells, Ana2 recruitment to centrioles occurs during late anaphase when mother–daughter pairs disengage, typically appearing as two spots that colocalize with each pericentrin-like protein (PLP)–labeled centriole ring: one spot positioned near the center of the PLP ring (presumably associated with the cartwheel) and a second spot near the periphery that marks the preprocentriole. Sas6 follows Ana2 to the preprocentriole, and this pattern persists into interphase (Dzhindzhev et al., 2017). To examine the effects of S38 phospho mutants on Ana2's centriole recruitment, we depleted endogenous Ana2 and used super resolution–structured illumination microscopy to localize transgenic GFP-Ana2 in interphase cells. Most centrioles in cells expressing transgenic Ana2-WT contained two Ana2 spots (75%); the remaining centrioles contained only the peripheral procentriole spot (Fig. 6, A and B). Interestingly, linescans of centrioles with two spots revealed an asymmetry in Ana2 levels. Specifically, the immunofluorescence intensity of Ana2 at the procentriole was, on average, twofold greater than the intensity of the Ana2 spot located within the mother centriole (Fig. 6 D). A similar pattern was observed in cells expressing PM Ana2-S38D: 68% of centrioles contained two spots of Ana2-S38D where the Ana2 spot on the procentriole was 2.2-fold more intense (Fig. 6, A–D). However, expression of phospho-null Ana2-S38A altered this pattern. Although some centrioles completely lacked Ana2-S38A (25%), most centrioles contained a single spot located in the center of the mother centriole instead of at the procentriole (46%; Fig. 6, B and C). Interestingly, linescans of centrioles containing two spots (25%) showed that Ana2-S38A levels were nearly equal at both sites (Fig. 6, A and D). A similar pattern was observed in cells expressing the Ana2 P11A/R12A mutant; only 38% of centrioles contained two spots of P11A/R12A and, in centrioles with only one spot, it localized within the mother centriole center (Fig. 6, A–C). We note that although the proportion of procentriolar P11A/R12A was reduced on centrioles containing two spots, this was not significantly different compared with centrioles containing two spots of WT or S38D Ana2 (Fig. 6 D). Based on our findings, we suggest that Ana2 loading may occur in stages. Initially, Ana2 interacts with Sas4 to accumulate at preprocentrioles at a relatively low basal level (as seen in the S38A), but, following phosphorylation of S38, further Ana2 accumulation on procentrioles is stimulated. Failure to accumulate sufficient Ana2 on procentrioles likely explains why the S38A and P11A/R12A mutants fail to rescue centriole duplication defects, as we and others previously reported (Cottee et al., 2013; Dzhindzhev et al., 2017; McLamarrah et al., 2018).

S38 phosphorylation increases Ana2 binding to the Sas4 G-box

Previous studies found human and zebrafish CPAP G-box bound to an NT ∼45–amino acid segment of STIL with a K_d of 0.6–2 µM (Cottee et al., 2013; Hatzopoulos et al., 2013). To examine the effects of Ana2 phosphorylation on Sas4 binding, we purified *Drosophila* Ana2 and Sas4 proteins from bacteria and used biolayer interferometry to measure their binding kinetics (Fig. S3). We found that an NT fragment (amino acids 1–60) of Ana2 bound the G-box with a K_d of 134 nM (Fig. 7 A and Fig. S3, B and E; see Materials and methods), which modestly increased in affinity (1.9-fold; K_d = 72 nM) when Ana2 1–60 was prephosphorylated with purified Plk4 (Fig. 7 A and Fig. S3, B and E). Interestingly, FL Ana2 bound Sas4 with a greater affinity (K_d = 26 nM) than the phospho-Ana2 1–60 fragment (Fig. 7 A and Fig. S3, C and E), again suggesting that additional Sas4-binding sites may be located outside the N terminus (Fig. 4 B). When FL Ana2 protein was prephosphorylated by Plk4, it displayed the tightest binding (K_d = 7 nM), an approximately fourfold increase compared with the nonphosphorylated protein (Fig. 7 A and Fig. S3, C and E). We next analyzed purified FL Ana2 containing the phospho-null S38A mutation. Notably, prephosphorylation with purified Plk4 caused the electrophoretic shift of WT Ana2 but not S38A (Fig. S3 A, right panel). Strikingly, prephosphorylation of the S38A mutant did not increase its affinity for the G-box because the K_d values for phospho-S38A (K_d = 28 nM), nonphospho-S38A (K_d = 31 nM), and WT Ana2 (K_d = 26 nM) were very similar (Fig. 7 A and Fig. S3, D and E). Thus, our findings suggest that the tightest G-box binding condition is achieved when Ana2 is FL and phosphorylated on S38. Our results do not exclude the possibility that additional phospho-Ana2 residues contribute to efficient G-box binding but do reveal that S38 is the key residue in mediating this interaction.

How does phosphorylation of S38 increase Ana2's binding affinity to Sas4? We previously showed that purified NT and C-terminal fragments of Ana2 bind in vitro, and their binding was maximal after the introduction of two clusters of PM mutations: two NT (NT-2PM) substitutions (T33E/S38D) and three C-terminal STAN domain (CT-3PM) substitutions (S318D/

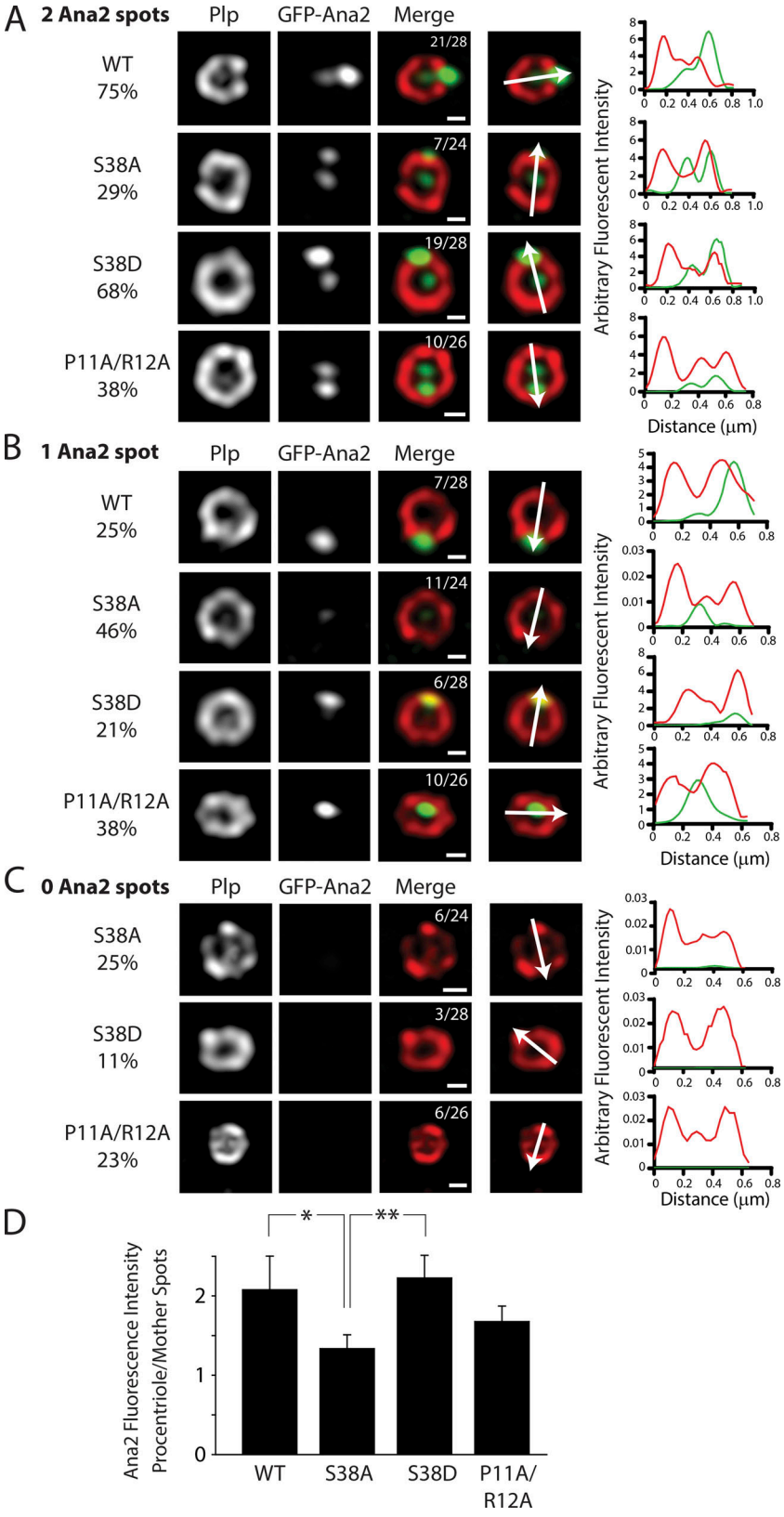

Figure 6. **WT and PM (S38D) Ana2 accumulate on procentrioles but the phospho-null Ana2-S38A mutant does not. (A–C)** Interphase centrioles in transgenic GFP-Ana2–expressing cells were imaged using super-resolution microscopy. S2 cells were depleted of endogenous Ana2 for 12 d by transfection of UTR dsRNA on days 0, 4, and 8. On days 4 and 8, cells were co-transfected with the indicated GFP-Ana2 constructs (green) and induced to express on day 5 by addition of 0.1 mM $CuSO_4$. On day 12, cells were immunostained with anti-PLP (red) to mark the surface of mature centrioles. DNA was visualized with Hoechst (not depicted). Images are grouped as centrioles possessing two (A), one (B), or no (C) Ana2 spots. Bars, 200 nm. Right: Graphs of PLP (red) and GFP-Ana2 (green) fluorescence intensities plotted against the length of a linescan (white arrow) spanning the diameter of an individual centriole. **(D)** Graph of Ana2 fluorescence intensity as a ratio of procentriole to mother centriole spots in centrioles containing two spots. Asterisks mark significant differences between treatments: *, $P < 0.05$; **, $P < 0.01$. Error bars, SEM; $n = 3$ experiments, ~5–12 centrioles per treatment.

S370D/S373D; McLamarrah et al., 2018). Moreover, super-resolution imaging of Ana2 within the cartwheel shows close proximity of its N and C termini, suggesting a folded confirmation (Gartenmann et al., 2017). Therefore, S38 phosphorylation may induce a structural change in Ana2, stabilizing a folded conformation with increased G-box binding affinity, possibly by exposing or clustering multiple binding sites. We used Iterative Threading Assembly Refinement (I-TASSER) structure

A

Protein	Sas4 G-box K_D (nM)
Ana2 1-60	134 ±1.3
pAna2 1-60	71.7 ± 1.5
Ana2 FL	25.5 ± 0.1
pAna2 FL	6.7 ± 0.02
Ana2 S38A FL	30.7 ± 0.2
pAna2 S38A FL	26.7 ± 0.3

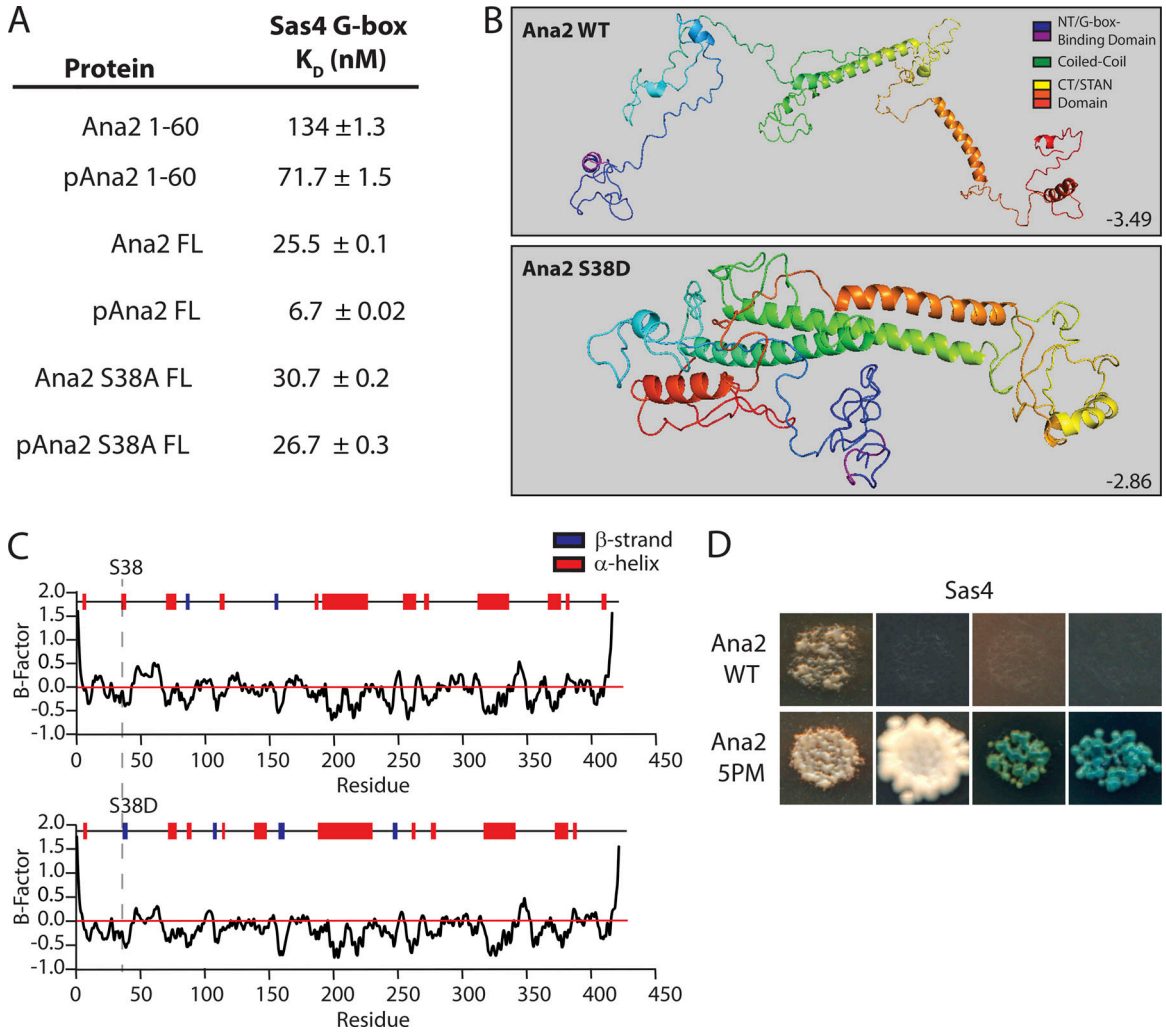

Figure 7. **Phosphorylation of Ana2 promotes stronger binding to Sas4 but not in the phospho-null S38A mutant. (A)** Calculated dissociation constants measured by bio-layer interferometry. Soluble WT Ana2 (FL or amino acids 1–60) or mutant S38A were either untreated or prephosphorylated by Plk4 and then incubated with probe-attached Sas4 G-box (amino acids 606–901; see Fig. S3 and Materials and methods). **(B)** I-TASSER protein structure predictions of WT (top) and S38D (bottom) Ana2. C-scores are shown. Note that the single S38D PM substitution is predicted to dramatically alter Ana2 conformation, folding Ana2 so that the N and C termini are closely positioned. **(C)** I-TASSER predictions of secondary structure within Ana2. The position of WT S38 (upper panel; dotted line) and PM S38D (lower panel) is indicated in a short segment that changes from an α-helix to a β-strand. **(D)** The PM (5PM) FL Ana2 construct interacts strongly with FL Sas4 by Y2H analysis. WT and 5PM Ana2 were screened against Sas4. In each image, colonies from replica plating are shown, and growth indicates the presence of bound bait and prey. From left to right: (1) no selection; (2) growth selection on QDO; growth and color selection on (3) DDOXA and (4) QDOXA (blue color indicates an interaction). See also section Y2H assay in Materials and methods.

prediction to examine how phosphorylation might affect Ana2 folding (Zhang, 2008; Roy et al., 2010, Yang et al., 2016). Unmodified Ana2 is largely disordered but contains five prominent α-helices of varying length (Fig. 7 B, top). However, a predicted conformation of Ana2 containing PM S38D shows a much different folded structure, with overlapping N and C termini (Fig. 7 B, bottom). Additionally, S38 lies within a 4-amino acid stretch (V37–L40) that is predicted to be an α-helix in the WT sequence but becomes a β-strand when containing the S38D substitution (Figs. 5 and 7). Remarkably, conformation modeling of NT-2PM, CT-3PM, and Ana2 containing all five substitutions (5PM) also predict a folded conformation with β-strand conversion of V37–L40 (Fig. S4). Since Ana2/STIL is a Cdk target (Campaner et al., 2005; Zitouni et al., 2016), we also modeled an Ana2 mutant containing Ser/Thr to Asp/Glu substitutions in all 12 of its possible Cdk consensus sites (12PM-Cdk), but this PM mutant did not predict a folded conformation (Fig. S4). Thus, our findings indicate that phosphorylation of the N terminus and STAN domain may promote both Ana2 folding and an interaction between the N and C termini, as well as alterations in secondary structure. These structural changes may account for the tighter binding of Ana2 with the Sas4 G-box.

Last, we inspected the Ana2–Sas4 interaction by Y2H. Curiously, no binding was detected between FL Ana2 and Sas4 (Fig. 7 D), possibly because the interaction of Sas4 with unmodified Ana2 is too weak to detect by Y2H. Therefore, we examined Ana2-5PM (which is predicted to have the most stably folded conformation; Fig. S4) and observed a strong interaction

between Sas4 and Ana2-5PM (Fig. 7 D), consistent with our in vitro binding experiments showing that FL phospho-Ana2 displays the strongest interaction with Sas4.

Discussion

The cartwheel protein Sas6 follows Ana2 to the procentriole assembly site. This event is prompted when Plk4 phosphorylates the Ana2/STIL STAN domain, generating a Sas6-binding surface that supports Sas6 aggregation at the procentriole assembly site (Dzhindzhev et al., 2014; Ohta et al., 2014; Kratz et al., 2015; Moyer et al., 2015). These seminal discoveries provided molecular insight into Plk4's role in initiating centriole duplication and characterized one of the earliest steps in the process. The goal of our study was to characterize the step prior, specifically, to understand how Ana2 is recruited to the preprocentriole, the single spot constructed on the surface of a mother centriole during mitotic exit in *Drosophila* cells (Dzhindzhev et al., 2017). We found that Ana2's centriolar recruitment is triggered by Ana2's interaction with Sas4, which leads to Ana2 phosphorylation by Plk4, tighter Sas4 binding, and, consequently, its accumulation on the procentriole assembly site.

Plk4 phosphorylation of Ana2 S38 is the key to understanding Ana2's centriole recruitment. S38 is one of the first Ana2 residues phosphorylated by Plk4 (McLamarrah et al., 2018), and the importance of this modification is underscored by the observation that phospho-null S38A fails to load onto most procentrioles and rescue centriole duplication (Fig. 6; Dzhindzhev et al., 2017; McLamarrah et al., 2018). Though Plk4 can phosphorylate Ana2 S38 in vitro in the absence of Sas4 (presumably due to the high concentrations of the reactants), the situation is more complex in cells, and our observations lead us to propose the following model (Fig. 8).

As cells exit mitosis and preprocentrioles form, Plk4 localizes to this site in an autoinhibited form, using its PB (PB1-PB2) domains to interact with the Sas4 G-box. Ana2 is an extended molecule (Fig. 8 A) when first recruited to the centriole surface, using a conserved proline-rich motif in its N terminus to bind the Sas4 G-box (Cottee et al., 2013; Hatzopoulos et al., 2013). Because the Sas4 G-box binds both Ana2 and Plk4 and stimulates the Plk4-dependent hyperphosphorylation of Ana2, the G-box functions as a multiplex binding platform that juxtaposes Ana2 and Plk4, thereby facilitating the phosphorylation of Ana2 S38 (Fig. 8, B and C). Future structural studies will be necessary to understand where PB1-PB2 binds the G-box, and if Ana2 and Plk4 can both occupy the G-box simultaneously. We acknowledge the many possible alternatives; for example, the G-box could be single-occupancy, and incoming Ana2 could displace G-box–bound Plk4, allowing Plk4 to interact with the immobilized Ana2. Indeed, binding between the Plk4 and Sas4 is relatively weak, explaining why this interaction is difficult to detect by IP. In this scenario, however, weak binding may allow an efficient "hand-off" of Plk4 to Ana2. Autoinhibited Plk4 is activated by its interaction with Ana2 and, in turn, Ana2 is phosphorylated on its N terminus (including S38) and then on its STAN domain (Fig. 8 C; McLamarrah et al., 2018).

S38 is a conserved residue in Ana2/STIL family members and, based on crystal structures of vertebrate STIL/CPAP complexes, is in contact with the Sas4 G-box (Cottee et al., 2013; Hatzopoulos et al., 2013). However, our findings suggest that S38 phosphorylation is structurally transformative, causing a localized change in secondary structure (Fig. 7, B and C), which may promote the stronger G-box binding that we observed (Fig. 7 A). Additional crystallographic studies of phospho (or PM)-Ana2 are needed to understand the structural basis of its tighter binding to the G-box; we predict that it does so through more than one G-box–binding domain. Further phosphorylation of the N and C termini promotes their interaction and, consequently, Ana2 adopts a folded conformation (Fig. 8 D). Tighter Sas4 binding by phospho-Ana2 (Fig. 7, A and D) enhances its accumulation at the future procentriole assembly site (Fig. 6). Because the preprocentriolar accumulation of Ana2 is important for centriole duplication, the relatively low binding affinity of phospho-null-Ana2 could explain why this mutant fails to support duplication (Dzhindzhev et al., 2017; McLamarrah et al., 2018). Measuring the turnover of Ana2 and its phospho-isoforms on the preprocentriole will be a challenging but important line of experimentation.

Last, our study identifies the first mechanistic function of the Ana2–G-box interaction. Previous studies demonstrated that this conserved interaction is required for centriole assembly and hypothesized that Ana2–G-box forms a functional "strut" within the pinhead of the cartwheel (Hiraki et al., 2007), thereby providing structural integrity to the organelle (Cottee et al., 2013; Hatzopoulos et al., 2013). Although this hypothesis is plausible, our findings show that this interaction plays a different critical step in the assembly process. Without the Ana2–G-box interaction, Plk4 cannot phosphorylate Ana2, likely because Ana2 fails to target preprocentrioles. In fact, when the P11A/R12A mutant is used to weaken the interaction with Sas4, Ana2 hyperphosphorylation is blocked and its normal accumulation on procentrioles is inhibited. Like Ana2, Sas4 is distributed as an asymmetric spot on centrioles in interphase *Drosophila* cells (Galletta et al., 2016). Determining how and when Sas4 acquires this pattern and whether Plk4 activity regulates its localization will be important future lines of investigation. Identifying additional upstream Plk4 phosphorylation targets is vital in unraveling the complex molecular choreography that underlies centriole assembly.

Materials and methods

Cell culture and double-stranded RNAi

Drosophila S2 cells (Drosophila Genomics Resource Center, S2-DRSC) were cultured in Sf-900II serum-free medium (Thermo Fisher Scientific, 10902088) at 25°C, normal air atmosphere, in nonventilated tissue culture–treated flasks. Double-stranded RNA (dsRNA) was synthesized in vitro from a dsDNA template (selected to target gene-specific sequence and bearing the T7 RNA polymerase promoter sequence [below] at each 5′ end) using purified T7 RNA polymerase, ribonucleoside triphosphates, and pyrophosphatase (Rogers and Rogers, 2008). To increase the efficiency of RNAi, S2 cells were transfected with dsRNA using program G-030

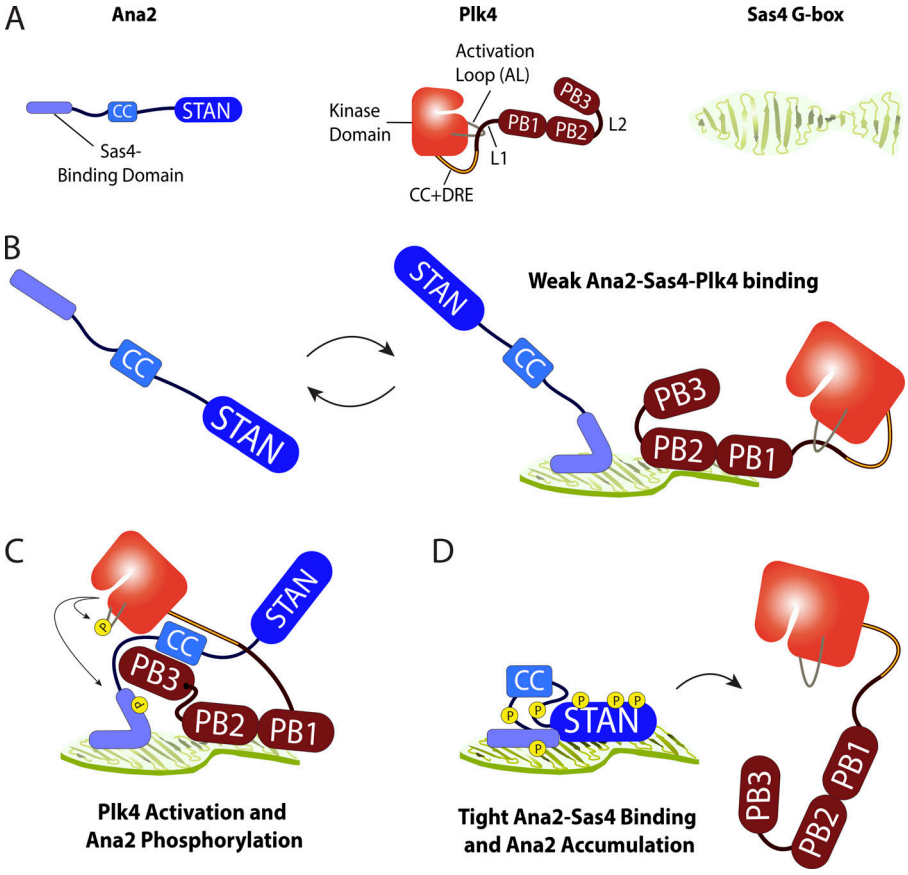

Figure 8. **Proposed model depicting the mechanism of Ana2 recruitment to the site of procentriole assembly. (A)** Schematics of Ana2, Plk4, and Sas4 showing structural and functional domains. Note that Plk4 initially exists in its autoinhibited form. Although these proteins homo-oligomerize, they are shown as monomers for simplicity. Only the C-terminal G-box domain of Sas4 is shown; it adopts an extended open β-sheet conformation. **(B)** During mitotic exit, unphosphorylated Ana2 (extended conformation) diffusing near a preprocentriole is weakly bound through its NT to one surface of the Sas4 G-box; substantial exchange of bound Ana2 with the cytoplasmic pool prevents sufficient accumulation at the preprocentriole to support centriole duplication. Plk4 also weakly binds the G-box through its PB1-PB2 cassette. **(C)** Ana2 binds and activates Plk4 by relieving its autoinhibition. In turn, active Plk4 phosphorylates the Ana2 NT, including S38, inducing Ana2 to fold. Subsequently, Plk4 phosphorylates the Ana2 STAN domain. During this step, Plk4 may be transferred from Sas4 to Ana2. **(D)** Phosphorylated NT and C-terminal domains of Ana2 bind one another and stabilize the folded conformation. Phospho-Ana2 binds tightly to the G-box through multiple contact sites. Tight binding to Sas4 allows Ana2 to accumulate on the preprocentriole, recruit Sas6, and promote centriole duplication. Further phosphorylation of the central domain in Ana2 causes Plk4 to release.

on a Nucleofector 2b electroporator (Lonza) and then were maintained in six-well plates (McLamarrah et al., 2018). For IP assays, 40 µg dsRNA was transfected on day 0 and 20 µg on day 4. For immunofluorescence microscopy and immunoblotting assays, cells were transfected with 40 µg dsRNA on days 0, 4, and 8.

Control dsRNA (~550 bp) was synthesized from DNA template amplified from noncoding sequence of the pET28a vector (Novagen, 69864-3) using the primers 5′-ATCAGGCGCTCTTCCGC-3′ and 5′-GTTCGTGCACACAGCCC-3′. (All primers used for dsRNA synthesis begin with the T7 promoter sequence 5′-TAATACGACTCACTATAGGG-3′, followed by target-specific sequence). dsRNA targeting Ana2 UTR was synthesized from a template made from EST LD22033 by first deleting the Ana2 cDNA, and then joining 91 bp of 5′ UTR with 78 bp of 3′ UTR; this construct was amplified using the primers 5′-CAGATTCTCCCGCTCG-3′ and 5′-TTCCGTGTATTGAAATATATTTCC-3′ to make the final template (McLamarrah et al., 2018). dsRNA targeting Sas4-UTR was synthesized from an oligonucleotide of fused Sas4 5′ UTR and 3′ UTR sequences (which includes the T7 RNA polymerase promoter sequence [in bold]): 5′-**TAATACGACTCACTATAGG**GCGTCTAAACAAAACTGCGATTCTAAGAACGAATATAAAAGCAGTCGGGTCTCTGCTTCCGTTGTTAAGTAAATTAACTTAAGTTTTAGATAAATAGCCCTATAGTGAGTCGTATTA-3′. The dsSas4-UTR template was generated by annealing equimolar complementary Sas4-UTR oligonucleotides at 95°C for 5 min in annealing buffer (10 mM Tris, pH 8.0, 50 mM NaCl, and 1 mM EDTA) followed by slow cooling to room temperature.

Immunoblotting

Cells were lysed in PBS–Triton X-100 (0.1%) followed by addition of SDS-PAGE loading buffer. Extracts were boiled for 5 min and stored at −20°C. Samples of equal total protein were resolved by SDS-PAGE, blotted, probed with primary and secondary antibodies, and scanned on an Odyssey CLX imager (Li-Cor Biosciences). For replacement experiments, cells were transfected with dsRNA on days 0, 4, and 8 to eliminate endogenous protein and were concurrently transfected with plasmids encoding protein constructs on days 4 and 8. Cells were induced to express transgenes with 0.1 mM $CuSO_4$ on day 5, maintained in 0.1 mM $CuSO_4$ for the duration of the experiment, and then analyzed on day 12. Primary antibodies used for Western blotting include rabbit anti-Ana2 (our laboratory), mouse HRP-conjugated anti-His_6 monoclonal (Thermo Fisher Scientific), rat anti-Sas4 (our laboratory), mouse anti-V5 monoclonal (Thermo Fisher Scientific, R96025), mouse anti-GFP monoclonal JL8 (Thermo Fisher Scientific, NC9777966), mouse anti-myc monoclonal (Cell Signaling Technologies, 2276S), and mouse anti-αtubulin monoclonal DM1A (Thermo Fisher Scientific, PI62204). Antibody dilutions ranged from 1:500 to 1:5,000. IRDye 800CW secondary antibodies (Li-Cor Biosciences; goat anti-mouse 92632210, goat anti-rat 92632219, goat anti-rabbit 92668021 [680LT]) were prepared according to the manufacturer's instructions and used at 1:3,000 dilution. Detection of fluorescent secondaries was performed using an Odyssey CLX imager (Li-Cor Biosciences). HRP-conjugated secondaries were

visualized by ECL with SuperSignal West Dura Extended Duration Substrate (Thermo Fisher Scientific, 34075) on a ChemiDoc MP Imaging System (Bio-Rad).

Immunofluorescence microscopy

S2 cells were spread on concanavalin A–coated glass-bottom plates and fixed in ice-cold methanol for 15 min. Cells were washed with PBS–Triton X-100 (0.1%) and then blocked in blocking buffer (5% normal goat serum in PBS–Triton X-100) for 30 min at room temperature. Samples were incubated at room temperature with rabbit anti-PLP (Rogers and Rogers, 2008) diluted at 1:3,000 in blocking buffer followed by three washes with PBS–Triton X-100. Cells were next incubated with Rhodamine red-X goat anti-rabbit secondary antibody (Jackson ImmunoResearch, 111-295-144) diluted 1:1,500 and with 3.2 µM Hoechst 33342 (Thermo Fisher Scientific, H3570) in blocking buffer, followed by three washes with PBS–Triton X-100, and then mounted in Vectashield (Vector Laboratories, H1000). Super-resolution microscopy was performed using a Zeiss ELYRA S1 (Super Resolution-Structured Illumination Microscopy) system equipped with an Axio Observer Z1 inverted microscope with transmitted tungsten halogen, UV mercury short arc lamp, and solid-state (405/488/561 nm) laser illumination sources, an Alpha Plan-APO 100× objective (NA 1.4), three rotations, and an EM–charge-coupled device camera (Andor iXon). Images were acquired with ZEN 2011 software. Statistical analysis of ratios of fluorescence intensities was performed using "one-tailed" tests because WT Ana2 spots were asymmetric, appearing brighter on procentrioles than in mother centrioles.

Constructs

FL cDNAs of *Drosophila* Ana2, Plk4, and Sas4 were subcloned into the pMT/V5-His vector (Thermo Fisher Scientific, V412020) containing in-frame coding sequences for EGFP, V5, or myc under control of the inducible metallothionein promoter. PCR-based site-directed mutagenesis with Phusion DNA polymerase (Thermo Fisher Scientific, F530) was used to generate the Ana2, Sas4, and Plk4 point mutants. Transgenic constructs were induced to express ∼24 h after transfection by the addition of 0.1–1 mM copper sulfate to the culture medium.

IP assays

GFP-binding protein (GBP; Rothbauer et al., 2008) was fused to the Fc domain of human IgG (pIg-Tail; R&D Systems), tagged with His_6 in pET28a (Novagen, 69864–3), expressed in *Escherichia coli*, and purified on HisPur Cobalt resin (Thermo Fisher Scientific, 89964; Buster et al., 2013). Purified His_6-tagged GBP-Fc or mouse anti-V5 monoclonal antibody (Thermo Fisher Scientific, R96025) was bound to magnetic Protein A Dynabeads (Thermo Fisher Scientific, 10002D), and then cross-linked to the resin by incubating with 20 mM dimethyl pimelimidate dihydrochloride in PBS, pH 8.3, for 2 h at 22°C. Then, the coupling reaction was quenched with 0.2 M ethanolamine, pH 8.3, for 1 h at 22°C. Antibody-coated beads were washed three times with PBS–Tween 20 (0.02%) and then equilibrated in 1.0 ml of cell lysis buffer (CLB; 50 mM Tris, pH 7.2, 125 mM NaCl, 2 mM DTT, 0.1% Triton X-100, 1× cOmplete EDTA-free protease inhibitor cocktail [Sigma-Aldrich, 11697498001], 0.1 mM PMSF, and 1× phosphatase inhibitor cocktail set 1 [Sigma-Aldrich, 524624]). For replacement experiments, cells were transfected with dsRNA on day 0, followed by concurrent transfection with 1–3 µg plasmid (encoding the exogenous construct) and 20 µg dsRNA on day 4. Expression of exogenous protein was induced with copper sulfate on day 5, and samples were collected on day 6. Transfected cells expressing recombinant proteins were lysed in CLB and the lysates clarified by centrifugation at 16,100 *g* for 5 min at 4°C. Transfected cell lysates were not precleared when preparing samples for mass spectrometry. 0.5–1% of the inputs were used for immunoblots. GBP-coated beads were rocked with lysates for 30 min at 4°C (or with anti-V5–coated beads for 10 min at 22°C), washed four times with 1 ml CLB, and boiled in SDS-PAGE loading buffer.

Protein purification and prephosphorylation

GST-Ana2 FL, S38A, and 1–60 (amino acids 1–60) were purified as previously described (McLamarrah et al., 2018). Briefly, GST-tagged Ana2 construct was bacterially expressed and then purified from clarified bacterial lysate using GST resin (Thermo Fisher Scientific, PI16100). Heat shock protein (HSP) was removed by equilibrating resin-bound GST-Ana2 in 10 column volumes (CV) of HSP buffer (50 mM Tris, pH 7.5, 50 mM KCl, 20 mM $MgCl_2$) followed by washing with 20 CV of HSP buffer containing 5mM ATP (Thermo Fisher Scientific, NC0380542). GST tag was removed from GST-Ana2 by incubating the resin-bound protein with PreScission Protease (GE Healthcare, 27084301) overnight at 4°C. Protease-cleaved protein was recovered in the column flow-through, and the material was then passed through new GST resin to remove any remaining GST-tagged protease and uncut GST-tagged Ana2. Samples were analyzed by SDS-PAGE.

His_6-Thrombin-Sas4-606 (amino acids 606–901) and His_6-FLAG-Plk4 (amino acids 1–317) were purified on HisPur Cobalt resin (Thermo Fisher Scientific, 89964). His_6-Thr-Sas4-606 was eluted from the resin with 200 mM imidazole in PBS and 1 mM DTT followed by concentration and buffer exchange (into PBS, 1 mM DTT) using Amicon Ultra spin concentrators (Sigma-Aldrich, UFC801024). His_6-FLAG-Plk4 1–317 was eluted similarly and exchanged into reaction buffer (40 mM Na-Hepes, pH 7.3, 150 mM NaCl, 5 mM $MgCl_2$, 1 mM DTT, and 10% [by volume] glycerol).

GST-Ana2 was phosphorylated before cleavage of the GST tag as follows. GST-Ana2 immobilized on GST resin was exchanged into reaction buffer and incubated with 20 µM purified His_6-FLAG-Plk4 1–317 and 100 µM ATP for 1 h at room temperature while shaking. To remove Plk4, the resin (with immobilized Ana2) was washed with 10 CV of wash buffer (PBS, 1 mM EGTA, 1 mM PMSF, 1 mM DTT, and 1 mM soybean trypsin inhibitor [Sigma-Aldrich, T9128]), then 10 CV of wash buffer containing an additional 500 mM NaCl, followed by another 20 CV of wash buffer. The GST tag was cleaved overnight as described above, releasing purified tagless Ana2.

pExpress-Dual screen for isolating soluble protein complexes

We developed a four-step high-throughput method to screen for stable, soluble binary protein complexes from a library of constructs via coexpression in *E. coli*.

Step 1: Design and cloning for pExpress-Dual screen

pExpress-Dual plasmid was constructed by PCR amplifying a cassette containing a TEV cleavage site (ENLYFQS) followed by the linker GGSGGGSGGGSG and EGFP coding sequence (without a start codon) with two stop codons (TAG-TAA), which was then cloned into pST39 (Addgene, 64009) between the T7 promoter and the T7 terminator using primers TEV-linker forward (F): 5′-CTCACTATAGGGAGACCAC AACGGTTTCCCGAAAACCTGTACT TCCAATCCggtggttct-3′ and GFP-Stop reverse (R): 5′-TCCTTT CGGGCTTTGTTAGCAGCCGGATCTTTACTACTTGTACAGCTC GTCCATGCCGAG-3′. To assemble the dual expression library, pExpress-Dual was amplified as two pieces: (1) pExpress A using primers L3F: 30 bp of gene-specific sequence for each gene/fragment and 5′-GAAAACCTGTACTTCCAATCCggtggttct-3′ and L4R: 5′-TTTATCAGCAATAAACCAGCCAGCAGGAAGTGCCGA-3′, and (2) pExpress B using primers L4F: 5′-AAAGTTGCAGGA CCACTACTGCGTTCGGCA-3′ and L1R: 5′-ATTTCTCCTCTT TAATTCTAGGTACCCGGGGGGAAACCGTTGTGGTCTCCCTAT AGTGAG-3′. Primers for gene A cloning include L1F: 5′-CCC GGGTACCTAGAATTAAAGAGGAGAAATTAAGCATGCACC ACCATCACCATCAT-3′ and L2R: 5′-TATTCGACTATAACTGGC CGTCGTTTTACATTA-3′ followed by 30 bp of gene-specific sequence. Primers for gene A cloning include L2F: 5′-TGTAAA ACGACGGCCAGTTATAGTCGAATAAAACAAGTGGCTAAGGAG GTTGT-3′ and L3R: 5′-agaaccaccGGATTGGAAGTACAGGTTTTC-3′. PCR products ≥1 kb were mixed at equimolar ratios and at 5× molar ratios for fragments <1 kb. 30 ng of pExpress B and 15 µl of master mix were added for each 5 µl of DNA mixture and incubated for 2 h at 50°C and transformed (Gibson, 2011).

Step 2: Bacterial protein expression

(A) Transformation. 1 µl of the plasmid library reaction mixture was added to 50 µl BL21(DE3)pLysS competent *E. coli* (Thermo Fisher Scientific, C606003), incubated for 20 min on ice, and heat-shocked for 1 min at 37°C. 300 µl of Luria broth (LB) was added to the mixture, placed in a 250 rpm shaker for 1 h at 37°C, plated on three agar plates supplemented with 100 µg/ml ampicillin, and incubated overnight at 37°C. (B) Colony expansion. 96 random colonies were inoculated into 96-well plates containing 100 µg/ml ampicillin and replicate plated on gridded LB ampicillin plates. (C) Bacterial growth and induction of protein expression. 1 ml of TB medium with ampicillin and 1% (vol/vol) glucose was added to each well. Plates were sealed with Parafilm and placed in a 250 rpm shaker at 37°C overnight. 100 µl of culture was diluted into a new 96-well plate containing 900 µl of supplemented TB medium per well, sealed, and incubated at 250 rpm at 37°C until cultures reached an OD_{600} = 1.0. Expression was induced by adding 0.5 mM IPTG per well, and plates were incubated at 250 rpm at 18°C overnight. Cells were harvested by centrifugation at 2,000 *g* at 4°C for 15 min, supernatants decanted, and plates stored at −80°C. (D) Purification of soluble protein complexes. 150 µl of lysis buffer was added to each well. Plates were placed in a shaker at 30°C for 30 min and then incubated on ice for 5 min. 50 µl of Benzonase buffer (all buffer recipes listed below) was added to each well and agitated at 4°C for 15 min. Lysates were clarified by centrifuging plates at 2,000 *g* for 15 min at 4°C. 50 µl of equilibration-binding buffer was added to each well, transferred to preequilibrated HisPur Ni-NTA Spin Plates (Thermo Fisher Scientific, 88230), sealed, and agitated at 4°C for 30–60 min. Plates were placed on a vacuum manifold, filtered using ∼4 inches Hg of pressure, and washed 3× with 200 µl of wash buffer, and the resin was resuspended in 100 µl of elution buffer. Plates were then sealed and incubated with gentle agitation at 4°C for 15 min. Holes were punched on either side of a clean 96-well collection plate, the filter plate and the collection plate were sealed, and eluate was collected by vacuum.

Step 3: Primary screening

2 µl of eluate from each well was transferred onto two nitrocellulose membranes. For GFP-immunoblotting protein detection, membranes were blocked with 5% milk in TBS containing 0.05% Tween-20 for 1 h at room temperature. For detection of His_6-tagged protein, membrane was blocked with 2.5% BSA in PBS containing 0.3% Triton X-100 for 1 h at room temperature.

Step 4: Secondary screening

False positives from the primary screen was identified by the following: (A) Single protein insertions that were double-tagged with His_6 on the N terminus and GFP on the C terminus were identified by PCR using T7 and M13F (-21) reverse primers that recognize flanking regions of gene A insertion sites. Any colony not producing PCR product was marked as a dual-tagged false positive. Following this step, 62 colonies remained. (B) Duplications were identified by sequence analysis, yielding 48 candidate dual expression vectors. (C) Tandem pulldown/IP for His_6 and GFP. For His_6 pulldowns, 25 ml overnight cultures were pelleted and resuspended in 1 ml of lysis buffer, incubated on ice for 5 min, and sonicated. Lysates were then precleared by centrifugation at 2,000 *g* for 15 min at 4°C. 25 µl (total bed volume) of equilibrated His-Tag Dynabeads (Thermo Fisher Scientific, 10103D) were added to supernatant and rocked for 15–30 min at 4°C. Beads were retrieved with a magnet, gently washed 3× with 300 µl wash buffer, and resuspended in 150 µl of elution buffer for 10 min at 4°C. For GFP IPs, 25 µl (total bed volume) of Protein A Dynabeads (Thermo Fisher Scientific, 10002D) were resuspended in 1 ml PBS + 0.01% Tween-20 with 0.5 µl of anti-GFP antibody (Abcam, ab290) and rocked for 30–60 min at 4°C. Proteins were eluted by resuspending beads in 25–50 µl of SDS-PAGE loading buffer (2×) and boiling for 8 min.

Buffer recipes for pExpress-Dual screen

The following buffer recipes were used: LB medium (1.0% tryptone, 0.5% yeast extract, and 1.0% NaCl); TB medium (1.2% tryptone, 2.4% yeast extract, 0.5% [vol/vol] glycerol, 0.17 M KH_2PO_4, and 0.72 M K_2HPO_4); lysis buffer (B-PER Bacterial Protein Extraction Reagent [Thermo Fisher Scientific, 78248], 150 mM NaCl, 10 mM 2-mercaptoethanol, 0.1 mM EDTA, 0.2 mg/ml lysozyme, 1 mM PMSF, and 1× cOmplete EDTA-free protease inhibitor cocktail [Sigma, 11697498001]); Benzonase buffer (50 mM Tris-HCl, pH 7.4, 1.2 mM $MgCl_2$, and 0.1 U/µl Benzonase); equilibration/binding buffer (50 mM Tris-HCl, pH 7.4, 150 mM NaCl, 5 mM imidazole, 10 mM 2-mercaptoethanol, 1 mM PMSF, and 1× cOmplete EDTA-free protease inhibitor

cocktail); wash buffer (50 mM Tris-HCl, pH 7.4, 150 mM NaCl, 10 mM imidazole, 10 mM 2-mercaptoethanol, 1 mM PMSF, and 1× cOmplete EDTA-free protease inhibitor cocktail); and elution buffer (50 mM Tris-HCl, pH 7.4, 150 mM NaCl, 300 mM imidazole, and 10 mM 2-mercaptoethanol).

MST

His_6-Plk4 PB1-PB2 (amino acids 382–602) and MBP Sas4 G-box (amino acids 708–901) were purified (using Ni-affinity or amylose resins, respectively), concentrated, and exchanged into PBS and 0.05% Tween-20. Although His_6-PB1-PB2 was not isolated to purity, we confirmed it was the only His_6-tagged species in the isolate by α-His_6 immunoblots (Fig. S4 A). His_6-PB1-PB2 was labeled using a Monolith NT His-Tag Labeling Kit RED-Tris-NTA (Nanotemper, MO-L008). MST was performed using standard capillaries in a Monolith NT.115 Blue/Red (Nanotemper) with a constant concentration of labeled His_6-Plk4 PB1-PB2 (50 nM) and a range of concentrations of MBP (control) and MBP-Sas4 G-box. Four technical replicates using MBP–G-box and two using MBP were performed. Capillaries showing highly aberrant MST curves, likely a result of pipetting errors or protein aggregation, were excluded (MBP-Sas4 G-box: excluded 5 of 64, MBP: 1 of 32). Results of the technical replicates were averaged to generate binding isotherms that were fit using MATLAB (MathWorks).

Bio-layer interferometry

Bio-layer interferometry data were collected on a Octet RED384 system (Pall ForteBio) using 96-well plates (Grenier, 655209). Kinetic assays were performed by first equilibrating Ni-NTA Octet biosensors (Molecular Devices, 18-5101) in kinetic buffer (PBS, 0.01% BSA, and 0.002% Tween-20) during a baseline step for 60 s, followed by loading with 8 µg/ml His_6-Thr-Sas4-606 in PBS and 1 mM DTT for 120 s. Sas4-coated biosensors were next equilibrated in sample buffer (PBS, 0.01% CHAPS, 1% BSA, and 10 mM imidazole) for 180 s in a second baseline step. Sas4-coated biosensors were then submerged in wells for 120 s containing different concentrations of either nonphosphorylated or prephosphorylated Ana2 FL, 1–60, or S38A (point mutant of FL). This association step was followed by a dissociation step for 300 s in sample buffer. Ni-NTA biosensors were regenerated using a 5-s regeneration step in 500 mM imidazole in PBS followed by a 5-s neutralization step in kinetic buffer. This process was repeated five times for complete regeneration of biosensors. The binding sensorgrams were collected using the eight-channel detection mode on the Octet RED384. Association and dissociation constants were calculated with Data Analysis 11.0 software (Pall ForteBio). Binding sensorgrams were globally fit to a 1:1 binding model following subtraction of a single reference set. (The 1:1 binding model probably does not accurately describe Ana2/Sas4 binding, but until future studies fully characterize Ana2/Sas4 binding, we have chosen to use the 1:1 model to obtain approximate K_d values in order to compare the relative affinities of the Ana2 constructs.) Data were aligned in the y axis to the average of the baseline step with an inter-step correction aligned to the dissociation step and filtered using Savitzky–Golay filtering. Graphs were generated using Prism 8 software (GraphPad).

Y2H assay

Y2H experiments were carried out using the Matchmaker Gold Y2H system (Clontech) with significant modifications. pDEST-GADT7 and pDEST-GBKT7, modified versions of Matchmaker vectors compatible with the Gateway cloning system (Life Technologies), were used (Rossignol et al., 2007). pDEST-GADT7 and pDEST-GBKT7 contain the 2 µ and pUC ori for growth in yeast and bacteria. Both contain the Gateway cassette and utilize the ADH1 promoter to drive expression in *Saccharomyces cerevisiae*. pDEST-GADT7 fuses the SV40 nuclear localization signal, the GAL4 activation domain, and the HA epitope tag to the N terminus of the protein encoded by DNA inserted into the Gateway cassette. pDEST-GBKT7 fuses the SV40 nuclear localization signal, the GAL4 DNA binding domain, and the c-Myc epitope tag to the N terminus of the protein encoded by DNA inserted into the Gateway cassette. pDest-pGBKT7 was modified by yeast-mediated recombination to confer resistance to ampicillin instead of kanamycin. pDEST-GADT7 and pDEST-GBKT7 plasmids containing fragments encoding the protein regions to be tested for interaction were transformed into Y187 and Y2HGold yeast strains, respectively, using standard techniques. Liquid cultures of yeast carrying these plasmids were grown at 30°C, with shaking, to an OD_{600} of ∼0.5 in SD – leu or SD – trp media, as appropriate, to maintain plasmid selection. Interactions were tested by mating, mixing 20 µl each of a Y187 strain and a Y2HGold strain in 100 µl of 2× YPD media in a 96-well plate. Mating cultures were grown for 20–24 h at 30°C with shaking. Cells were pinned onto SD – leu – trp (DDO) plates to select for diploids carrying both plasmids, using a Multi-Blot Replicator (VP 407AH, V&P Scientific), and grown for 5 d at 30°C. These plates were then replica plated onto DDO, SD – ade – leu – trp – ura (QDO), SD – leu – trp + aureobasidin A (Clontech) + X-α-Gal (Clontech, Gold Biotechnology; DDOXA), and/or SD – ade – leu – trp – ura + aureobasidin A + X-α-Gal (QDOXA). Replica plates were grown for 5 d at 30oC. Interactions were scored based on growth and/or blue color, as appropriate.

In silico structural analysis

FL Ana2 WT or Ana2 mutant sequence files were analyzed using I-TASSER for protein structure and function prediction (Zhang, 2008; Roy et al., 2010; Yang et al., 2016). Using I-TASSER, five models were predicted for each construct and an optimal model was selected for each construct based on C-score and known structural features. The normalized B-factor (B-factor profile, a measure of fluctuations of atoms around their average positions) is predicted by the I-TASSER algorithm using a template-based and profile-based prediction (Yang et al., 2016).

Mass spectrometry

S2 cells expressing transgenic Ana2 were solubilized in CLB, and tagged Ana2 was purified either by IP (using anti-V5) or pull-down (using purified GBP-Fc). Samples were further resolved by SDS-PAGE, and selected regions of the Coomassie-stained gels were collected. After destaining, gel pieces were reduced (10 mM DTT in 25 mM NH_4HCO_3, 55°C, 60 min), alkylated (55 mM iodoacetamide in 25 mM NH_4HCO_3, 45 min, in the dark at room temperature), and proteolyzed (1.5 µg chymotrypsin,

0.6 µg trypsin in 50 mM NH_4HCO_3, and 1 mM $CaCl_2$, overnight at room temperature, and then 2 h at 37°C). Peptides were extracted from the gel pieces (using a series of 20 min incubations at 37°C in 1% trifluoroacetic acid and increasing [25–99%] acetonitrile), dried, and resuspended in 0.1% trifluoroacetic acid, and then desalted with NuTip carbon micro-cartridges (Glygen, NT2CAR). Processed samples were stored at −20°C until analyzed.

Liquid chromatography MS/MS analysis was performed using a Q Exactive Plus mass spectrometer (Thermo Fisher Scientific) equipped with a nanoESI source. The nanoLC was a Dionex Ultimate 3000 RSLCnano System (Thermo Fisher Scientific). Peptides were loaded onto an Acclaim PepMap 100 trap column (75 µm inner diameter [ID] × 25 cm; Thermo Fisher Scientific, 164569) for 10 min at 3 µl/min, then eluted onto an Acclaim PepMap RSLC C18 analytical column (75 µm ID × 25 cm; Thermo Fisher Scientific, 164536) using a 5–20% gradient of solvent B (acetonitrile, 0.1% formic acid) over 122 min, 20–50% solvent B over 10 min, 50–95% of solvent B over 10 min, 95% hold of solvent B for 10 min, and finally a return to 5% solvent B in 1 min and another 10-min hold of 5% solvent B. Solvent A consisted of water and 0.1% formic acid. The flow rate on the analytical column was 300 nl/min. Spectral data were acquired using a Data Dependent scanning by Xcalibur software version 4.0.27.19 (Andon et al., 2002), using a survey scan at 70,000 resolution scanning mass/charge (m/z) 353–1,550 at an automatic gain control target of 10^5 and a maximum injection time of 65 ms, followed by higher-energy collisional dissociation MS/MS at 27 normalized collision energy of the 10 most intense ions at a resolution of 17,500, an isolation width of 1.5 m/z, an automatic gain control of 10^5, and a maximum injection time of 65 ms. Dynamic exclusion was set to place any selected m/z on an exclusion list for 20 s after a single MS/MS. Ions of charge state +1, 7, 8, >8, and unassigned were excluded from MS/MS, as were isotopes. Tandem mass spectra were searched against a *Drosophila* proteome Uniprot database to which common contaminant protein (e.g., chymotrypsin, trypsin, keratins; obtained at ftp://ftp.thegpm.org/fasta/cRAP) and the transfected construct sequences were appended. All MS/MS spectra were searched using Thermo Proteome Discoverer v2.2.0388 (Thermo Fisher Scientific) considering fully proteolyzed peptides with up to two missed cleavage sites. Variable modifications considered during the search included methionine oxidation (15.995 D), cysteine carbamidomethylation (57.021 D), and phosphorylation (79.99 D) of serine, threonine, and tyrosine. Proteins were identified at 99% confidence with XCorr score cut-offs (Qian et al., 2005) as determined by a reversed database search. The protein and peptide identification results were also visualized with Scaffold Q+S version 4.8.7 (Proteome Software), which relies on the Sequest search engine results and uses Bayesian statistics to reliably identify more spectra (Keller et al., 2002). Assignment of the phospho-sites listed in Table S2 was performed with Scaffold PTM software (Proteome Software); S38, S63, and S150 of Ana2 expressed in S2 cells (coexpressing transgenic Sas4) were identified as phospho-sites with high confidence (Ascore > 18). However, the site assignments of the S150-containing phosphopeptides obtained from the control samples were low confidence (i.e., Ascore < 18), so the actual position of the single phosphate moiety within these particular phosphopeptides is unknown. We report the phosphopeptide sequences with the largest Ascores.

Online supplemental material

Figs. S1 and S2 show workflows of the primary and secondary binary complex screens, respectively. Fig. S3 shows the purified proteins used in the bio-layer interferometry assay and data from those experiments. Fig. S4 shows protein structure predictions for different Ana2 mutants. The immunoblot PDF shows the raw immunoblots from the tandem pulldown/IP step of the binary complex screen. Table S1 lists primers used in constructing the pExpress vectors for the protein-binding screen. Table S2 lists Ana2 phospho-sites identified by MS/MS in this study.

Acknowledgments

We thank S. Smith for help confirming Plk4-Sas4 interactions, A. Kelly for help with screen design, and G. Piszczek and D. Wu (National Heart, Lung, and Blood Institute Biophysics Core) for assistance with MST experiments and analysis.

This work was supported by the Division of Intramural Research at the National Institutes of Health/National Heart, Lung, and Blood Institute (1ZIAHL006104) to N.M. Rusan. G.C. Rogers is grateful for support from National Cancer Institute P30 CA23074 and National Institute of General Medical Sciences R01s GM110166 and GM126035 as well as National Institutes of Health grant 1S10OD019948-0.

The authors declare no competing financial interests.

Author contributions: T.A. McLamarrah designed, performed, and analyzed all experiments involving cultured fly cells and worked collaboratively with J.M. Ryniawec in performing the bio-layer interferometry experiments. S. Speed, C.J. Fagerstrom, and N.M. Rusan designed, performed, and analyzed all experimental work with protein-binding screens. D.W. Buster performed mass spectrometry experiments and edited the manuscript. B.J. Galletta performed microscale thermophoresis experiments. G.C. Rogers contributed to project design and manuscript preparation along with N.M. Rusan.

Submitted: 22 May 2019
Revised: 24 October 2019
Accepted: 12 November 2019

References

Andon, N.L., S. Hollingworth, A. Koller, A.J. Greenland, J.R. Yates III, and P.A. Haynes. 2002. Proteomic characterization of wheat amyloplasts using identification of proteins by tandem mass spectrometry. *Proteomics*. 2: 1156–1168. https://doi.org/10.1002/1615-9861(200209)2:9<1156::AID-PROT1156>3.0.CO;2-4

Arquint, C., A.M. Gabryjonczyk, S. Imseng, R. Böhm, E. Sauer, S. Hiller, E.A. Nigg, and T. Maier. 2015. STIL binding to Polo-box 3 of PLK4 regulates centriole duplication. *eLife*. 4:e07888. https://doi.org/10.7554/eLife.07888

Banterle, N., and P. Gönczy. 2017. Centriole biogenesis: from identifying the characters to understanding the plot. *Annu. Rev. Cell Dev. Biol.* 33:23–49. https://doi.org/10.1146/annurev-cellbio-100616-060454

Bettencourt-Dias, M., A. Rodrigues-Martins, L. Carpenter, M. Riparbelli, L. Lehmann, M.K. Gatt, N. Carmo, F. Balloux, G. Callaini, and D.M. Glover. 2005. SAK/PLK4 is required for centriole duplication and flagella development. *Curr. Biol.* 15:2199–2207. https://doi.org/10.1016/j.cub.2005.11.042

Bond, J., E. Roberts, K. Springell, S.B. Lizarraga, S. Scott, J. Higgins, D.J. Hampshire, E.E. Morrison, G.F. Leal, E.O. Silva, et al. 2005. A centrosomal mechanism involving CDK5RAP2 and CENPJ controls brain size. *Nat. Genet.* 37:353–355. https://doi.org/10.1038/ng1539

Buster, D.W., S.G. Daniel, H.Q. Nguyen, S.L. Windler, L.C. Skwarek, M. Peterson, M. Roberts, J.H. Meserve, T. Hartl, J.E. Klebba, et al. 2013. SCFSlimb ubiquitin ligase suppresses condensin II-mediated nuclear reorganization by degrading Cap-H2. *J. Cell Biol.* 201:49–63. https://doi.org/10.1083/jcb.201207183

Campaner, S., P. Kaldis, S. Izraeli, and I.R. Kirsch. 2005. Sil phosphorylation in a Pin1 binding domain affects the duration of the spindle checkpoint. *Mol. Cell. Biol.* 25:6660–6672. https://doi.org/10.1128/MCB.25.15.6660-6672.2005

Cizmecioglu, O., M. Arnold, R. Bahtz, F. Settele, L. Ehret, U. Haselmann-Weiss, C. Antony, and I. Hoffmann. 2010. Cep152 acts as a scaffold for recruitment of Plk4 and CPAP to the centrosome. *J. Cell Biol.* 191:731–739. https://doi.org/10.1083/jcb.201007107

Conduit, P.T., A. Wainman, and J.W. Raff. 2015. Centrosome function and assembly in animal cells. *Nat. Rev. Mol. Cell Biol.* 16:611–624. https://doi.org/10.1038/nrm4062

Cottee, M.A., N. Muschalik, Y.L. Wong, C.M. Johnson, S. Johnson, A. Andreeva, K. Oegema, S.M. Lea, J.W. Raff, and M. van Breugel. 2013. Crystal structures of the CPAP/STIL complex reveal its role in centriole assembly and human microcephaly. *eLife.* 2:e01071. https://doi.org/10.7554/eLife.01071

Cutts, E.E., A. Inglis, P.J. Stansfeld, I. Vakonakis, and G.N. Hatzopoulos. 2015. The centriolar protein CPAP G-box: an amyloid fibril in a single domain. *Biochem. Soc. Trans.* 43:838–843. https://doi.org/10.1042/BST20150082

Dzhindzhev, N.S., Q.D. Yu, K. Weiskopf, G. Tzolovsky, I. Cunha-Ferreira, M. Riparbelli, A. Rodrigues-Martins, M. Bettencourt-Dias, G. Callaini, and D.M. Glover. 2010. Asterless is a scaffold for the onset of centriole assembly. *Nature.* 467:714–718. https://doi.org/10.1038/nature09445

Dzhindzhev, N.S., G. Tzolovsky, Z. Lipinszki, S. Schneider, R. Lattao, J. Fu, J. Debski, M. Dadlez, and D.M. Glover. 2014. Plk4 phosphorylates Ana2 to trigger Sas6 recruitment and procentriole formation. *Curr. Biol.* 24:2526–2532. https://doi.org/10.1016/j.cub.2014.08.061

Dzhindzhev, N.S., G. Tzolovsky, Z. Lipinszki, M. Abdelaziz, J. Debski, M. Dadlez, and D.M. Glover. 2017. Two-step phosphorylation of Ana2 by Plk4 is required for the sequential loading of Ana2 and Sas6 to initiate procentriole formation. *Open Biol.* 7:170247. https://doi.org/10.1098/rsob.170247

Fu, J., and D.M. Glover. 2012. Structured illumination of the interface between centriole and peri-centriolar material. *Open Biol.* 2:120104. https://doi.org/10.1098/rsob.120104

Fu, J., Z. Lipinszki, H. Rangone, M. Min, C. Mykura, J. Chao-Chu, S. Schneider, N.S. Dzhindzhev, M. Gottardo, M.G. Riparbelli, et al. 2016. Conserved molecular interactions in centriole-to-centrosome conversion. *Nat. Cell Biol.* 18:87–99. https://doi.org/10.1038/ncb3274

Galletta, B.J., C.J. Fagerstrom, T.A. Schoborg, T.A. McLamarrah, J.M. Ryniawec, D.W. Buster, K.C. Slep, G.C. Rogers, and N.M. Rusan. 2016. A centrosome interactome provides insight into organelle assembly and reveals a non-duplication role for Plk4. *Nat. Commun.* 7:12476. https://doi.org/10.1038/ncomms12476

Gartenmann, L., A. Wainman, M. Qurashi, R. Kaufmann, S. Schubert, J.W. Raff, and I.M. Dobbie. 2017. A combined 3D-SIM/SMLM approach allows centriole proteins to be localized with a precision of ∼4-5 nm. *Curr. Biol.* 27:R1054–R1055. https://doi.org/10.1016/j.cub.2017.08.009

Gibson, D.G. 2011. Enzymatic assembly of overlapping DNA fragments. *Methods Enzymol.* 498:349–361. https://doi.org/10.1016/B978-0-12-385120-8.00015-2

Goshima, G., R. Wollman, S.S. Goodwin, N. Zhang, J.M. Scholey, R.D. Vale, and N. Stuurman. 2007. Genes required for mitotic spindle assembly in Drosophila S2 cells. *Science.* 316:417–421. https://doi.org/10.1126/science.1141314

Habedanck, R., Y.D. Stierhof, C.J. Wilkinson, and E.A. Nigg. 2005. The Polo kinase Plk4 functions in centriole duplication. *Nat. Cell Biol.* 7:1140–1146. https://doi.org/10.1038/ncb1320

Hatch, E.M., A. Kulukian, A.J. Holland, D.W. Cleveland, and T. Stearns. 2010. Cep152 interacts with Plk4 and is required for centriole duplication. *J. Cell Biol.* 191:721–729. https://doi.org/10.1083/jcb.201006049

Hatzopoulos, G.N., M.C. Erat, E. Cutts, K.B. Rogala, L.M. Slater, P.J. Stansfeld, and I. Vakonakis. 2013. Structural analysis of the G-box domain of the microcephaly protein CPAP suggests a role in centriole architecture. *Structure.* 21:2069–2077. https://doi.org/10.1016/j.str.2013.08.019

Hiraki, M., Y. Nakazawa, R. Kamiya, and M. Hirono. 2007. Bld10p constitutes the cartwheel-spoke tip and stabilizes the 9-fold symmetry of the centriole. *Curr. Biol.* 17:1778–1783. https://doi.org/10.1016/j.cub.2007.09.021

Holland, A.J., W. Lan, S. Niessen, H. Hoover, and D.W. Cleveland. 2010. Polo-like kinase 4 kinase activity limits centrosome overduplication by autoregulating its own stability. *J. Cell Biol.* 188:191–198. https://doi.org/10.1083/jcb.200911102

Hsu, W.B., L.Y. Hung, C.J. Tang, C.L. Su, Y. Chang, and T.K. Tang. 2008. Functional characterization of the microtubule-binding and -destabilizing domains of CPAP and d-SAS-4. *Exp. Cell Res.* 314:2591–2602. https://doi.org/10.1016/j.yexcr.2008.05.012

Hung, L.Y., H.L. Chen, C.W. Chang, B.R. Li, and T.K. Tang. 2004. Identification of a novel microtubule-destabilizing motif in CPAP that binds to tubulin heterodimers and inhibits microtubule assembly. *Mol. Biol. Cell.* 15:2697–2706. https://doi.org/10.1091/mbc.e04-02-0121

Ito, D., and M. Bettencourt-Dias. 2018. Centrosome remodelling in evolution. *Cells.* 7:E71. https://doi.org/10.3390/cells7070071

Jerabek-Willemsen, M., C.J. Wienken, D. Braun, P. Baaske, and S. Duhr. 2011. Molecular interaction studies using microscale thermophoresis. *Assay Drug Dev. Technol.* 9:342–353. https://doi.org/10.1089/adt.2011.0380

Keller, A., A.I. Nesvizhskii, E. Kolker, and R. Aebersold. 2002. Empirical statistical model to estimate the accuracy of peptide identifications made by MS/MS and database search. *Anal. Chem.* 74:5383–5392. https://doi.org/10.1021/ac025747h

Kim, T.S., J.E. Park, A. Shukla, S. Choi, R.N. Murugan, J.H. Lee, M. Ahn, K. Rhee, J.K. Bang, B.Y. Kim, et al. 2013. Hierarchical recruitment of Plk4 and regulation of centriole biogenesis by two centrosomal scaffolds, Cep192 and Cep152. *Proc. Natl. Acad. Sci. USA.* 110:E4849–E4857. https://doi.org/10.1073/pnas.1319656110

Klebba, J.E., D.W. Buster, T.A. McLamarrah, N.M. Rusan, and G.C. Rogers. 2015. Autoinhibition and relief mechanism for Polo-like kinase 4. *Proc. Natl. Acad. Sci. USA.* 112:E657–E666. https://doi.org/10.1073/pnas.1417967112

Kleylein-Sohn, J., J. Westendorf, M. Le Clech, R. Habedanck, Y.D. Stierhof, and E.A. Nigg. 2007. Plk4-induced centriole biogenesis in human cells. *Dev. Cell.* 13:190–202. https://doi.org/10.1016/j.devcel.2007.07.002

Kratz, A.S., F. Bärenz, K.T. Richter, and I. Hoffmann. 2015. Plk4-dependent phosphorylation of STIL is required for centriole duplication. *Biol. Open.* 4:370–377. https://doi.org/10.1242/bio.201411023

Lawo, S., M. Hasegan, G.D. Gupta, and L. Pelletier. 2012. Subdiffraction imaging of centrosomes reveals higher-order organizational features of pericentriolar material. *Nat. Cell Biol.* 14:1148–1158. https://doi.org/10.1038/ncb2591

McLamarrah, T.A., D.W. Buster, B.J. Galletta, C.J. Boese, J.M. Ryniawec, N.A. Hollingsworth, A.E. Byrnes, C.W. Brownlee, K.C. Slep, N.M. Rusan, and G.C. Rogers. 2018. An ordered pattern of Ana2 phosphorylation by Plk4 is required for centriole assembly. *J. Cell Biol.* 217:1217–1231. https://doi.org/10.1083/jcb.201605106

Mennella, V., B. Keszthelyi, K.L. McDonald, B. Chhun, F. Kan, G.C. Rogers, B. Huang, and D.A. Agard. 2012. Subdiffraction-resolution fluorescence microscopy reveals a domain of the centrosome critical for pericentriolar material organization. *Nat. Cell Biol.* 14:1159–1168. https://doi.org/10.1038/ncb2597

Mennella, V., D.A. Agard, B. Huang, and L. Pelletier. 2014. Amorphous no more: subdiffraction view of the pericentriolar material architecture. *Trends Cell Biol.* 24:188–197. https://doi.org/10.1016/j.tcb.2013.10.001

Moyer, T.C., K.M. Clutario, B.G. Lambrus, V. Daggubati, and A.J. Holland. 2015. Binding of STIL to Plk4 activates kinase activity to promote centriole assembly. *J. Cell Biol.* 209:863–878. https://doi.org/10.1083/jcb.201502088

Nigg, E.A., and A.J. Holland. 2018. Once and only once: mechanisms of centriole duplication and their deregulation in disease. *Nat. Rev. Mol. Cell Biol.* 19:297–312. https://doi.org/10.1038/nrm.2017.127

Novak, Z.A., P.T. Conduit, A. Wainman, and J.W. Raff. 2014. Asterless licenses daughter centrioles to duplicate for the first time in Drosophila embryos. *Curr. Biol.* 24:1276–1282. https://doi.org/10.1016/j.cub.2014.04.023

Ohta, M., T. Ashikawa, Y. Nozaki, H. Kozuka-Hata, H. Goto, M. Inagaki, M. Oyama, and D. Kitagawa. 2014. Direct interaction of Plk4 with STIL

ensures formation of a single procentriole per parental centriole. *Nat. Commun.* 5:5267. https://doi.org/10.1038/ncomms6267

Ohta, M., K. Watanabe, T. Ashikawa, Y. Nozaki, S. Yoshiba, A. Kimura, and D. Kitagawa. 2018. Bimodal binding of STIL to Plk4 controls proper centriole copy number. *Cell Reports.* 23:3160–3169.e4. https://doi.org/10.1016/j.celrep.2018.05.030

Peel, N., N.R. Stevens, R. Basto, and J.W. Raff. 2007. Overexpressing centriole-replication proteins in vivo induces centriole overduplication and de novo formation. *Curr. Biol.* 17:834–843. https://doi.org/10.1016/j.cub.2007.04.036

Qian, W.J., T. Liu, M.E. Monroe, E.F. Strittmatter, J.M. Jacobs, L.J. Kangas, K. Petritis, D.G. Camp II, and R.D. Smith. 2005. Probability-based evaluation of peptide and protein identifications from tandem mass spectrometry and SEQUEST analysis: the human proteome. *J. Proteome Res.* 4:53–62. https://doi.org/10.1021/pr0498638

Robbins, E., G. Jentzsch, and A. Micali. 1968. The centriole cycle in synchronized HeLa cells. *J. Cell Biol.* 36:329–339. https://doi.org/10.1083/jcb.36.2.329

Rodrigues-Martins, A., M. Riparbelli, G. Callaini, D.M. Glover, and M. Bettencourt-Dias. 2007. Revisiting the role of the mother centriole in centriole biogenesis. *Science.* 316:1046–1050. https://doi.org/10.1126/science.1142950

Rogers, S.L., and G.C. Rogers. 2008. Culture of Drosophila S2 cells and their use for RNAi-mediated loss-of-function studies and immunofluorescence microscopy. *Nat. Protoc.* 3:606–611. https://doi.org/10.1038/nprot.2008.18

Rossignol, P., S. Collier, M. Bush, P. Shaw, and J.H. Doonan. 2007. Arabidopsis POT1A interacts with TERT-V(I8), an N-terminal splicing variant of telomerase. *J. Cell Sci.* 120:3678–3687.

Rothbauer, U., K. Zolghadr, S. Muyldermans, A. Schepers, M.C. Cardoso, and H. Leonhardt. 2008. A versatile nanotrap for biochemical and functional studies with fluorescent fusion proteins. *Mol. Cell. Proteomics.* 7:282–289. https://doi.org/10.1074/mcp.M700342-MCP200

Roy, A., A. Kucukural, and Y. Zhang. 2010. I-TASSER: a unified platform for automated protein structure and function prediction. *Nat. Protoc.* 5:725–738. https://doi.org/10.1038/nprot.2010.5

Sharma, A., A. Aher, N.J. Dynes, D. Frey, E.A. Katrukha, R. Jaussi, I. Grigoriev, M. Croisier, R.A. Kammerer, A. Akhmanova, et al. 2016. Centriolar CPAP/SAS-4 imparts slow processive microtubule growth. *Dev. Cell.* 37:362–376. https://doi.org/10.1016/j.devcel.2016.04.024

Slevin, L.K., J. Nye, D.C. Pinkerton, D.W. Buster, G.C. Rogers, and K.C. Slep. 2012. The structure of the plk4 cryptic polo box reveals two tandem polo boxes required for centriole duplication. *Structure.* 20:1905–1917. https://doi.org/10.1016/j.str.2012.08.025

Slevin, L.K., E.M. Romes, M.G. Dandulakis, and K.C. Slep. 2014. The mechanism of dynein light chain LC8-mediated oligomerization of the Ana2 centriole duplication factor. *J. Biol. Chem.* 289:20727–20739. https://doi.org/10.1074/jbc.M114.576041

Sonnen, K.F., L. Schermelleh, H. Leonhardt, and E.A. Nigg. 2012. 3D-structured illumination microscopy provides novel insight into architecture of human centrosomes. *Biol. Open.* 1:965–976. https://doi.org/10.1242/bio.20122337

Sonnen, K.F., A.M. Gabryjonczyk, E. Anselm, Y.D. Stierhof, and E.A. Nigg. 2013. Human Cep192 and Cep152 cooperate in Plk4 recruitment and centriole duplication. *J. Cell Sci.* 126:3223–3233. https://doi.org/10.1242/jcs.129502

Stevens, N.R., J. Dobbelaere, K. Brunk, A. Franz, and J.W. Raff. 2010. Drosophila Ana2 is a conserved centriole duplication factor. *J. Cell Biol.* 188:313–323. https://doi.org/10.1083/jcb.200910016

Tang, C.J., S.Y. Lin, W.B. Hsu, Y.N. Lin, C.T. Wu, Y.C. Lin, C.W. Chang, K.S. Wu, and T.K. Tang. 2011. The human microcephaly protein STIL interacts with CPAP and is required for procentriole formation. *EMBO J.* 30:4790–4804. https://doi.org/10.1038/emboj.2011.378

Thornton, G.K., and C.G. Woods. 2009. Primary microcephaly: do all roads lead to Rome? *Trends Genet.* 25:501–510. https://doi.org/10.1016/j.tig.2009.09.011

Varadarajan, R., and N.M. Rusan. 2018. Bridging centrioles and PCM in proper space and time. *Essays Biochem.* 62:793–801. https://doi.org/10.1042/EBC20180036

Vulprecht, J., A. David, A. Tibelius, A. Castiel, G. Konotop, F. Liu, F. Bestvater, M.S. Raab, H. Zentgraf, S. Izraeli, and A. Krämer. 2012. STIL is required for centriole duplication in human cells. *J. Cell Sci.* 125:1353–1362. https://doi.org/10.1242/jcs.104109

Wang, W.J., R.K. Soni, K. Uryu, and M.F. Tsou. 2011. The conversion of centrioles to centrosomes: essential coupling of duplication with segregation. *J. Cell Biol.* 193:727–739. https://doi.org/10.1083/jcb.201101109

Yang, J., Y. Wang, and Y. Zhang. 2016. ResQ: An approach to unified estimation of B-Factor and residue-specific error in protein structure prediction. *J. Mol. Biol.* 428:693–701. https://doi.org/10.1016/j.jmb.2015.09.024

Zhang, Y. 2008. I-TASSER server for protein 3D structure prediction. *BMC Bioinformatics.* 9:40. https://doi.org/10.1186/1471-2105-9-40

Zheng, X., L.M. Gooi, A. Wason, E. Gabriel, N.Z. Mehrjardi, Q. Yang, X. Zhang, A. Debec, M.L. Basiri, T. Avidor-Reiss, et al. 2014. Conserved TCP domain of Sas-4/CPAP is essential for pericentriolar material tethering during centrosome biogenesis. *Proc. Natl. Acad. Sci. USA.* 111:E354–E363. https://doi.org/10.1073/pnas.1317535111

Zheng, X., A. Ramani, K. Soni, M. Gottardo, S. Zheng, L. Ming Gooi, W. Li, S. Feng, A. Mariappan, A. Wason, et al. 2016. Molecular basis for CPAP-tubulin interaction in controlling centriolar and ciliary length. *Nat. Commun.* 7:11874. https://doi.org/10.1038/ncomms11874

Zitouni, S., M.E. Francia, F. Leal, S. Montenegro Gouveia, C. Nabais, P. Duarte, S. Gilberto, D. Brito, T. Moyer, S. Kandels-Lewis, et al. 2016. CDK1 prevents unscheduled PLK4-STIL complex assembly in centriole biogenesis. *Curr. Biol.* 26:1127–1137. https://doi.org/10.1016/j.cub.2016.03.055